ABSTRACT

KUMMERER, THERESA. Investigation of the Transient Regions of Multi-Source Pulsed RF Capacitively Coupled Plasma Discharges. (Under the direction of Steven Shannon.)

Pulsed plasmas have demonstrated tremendous promise for extending plasma applications. Pulsed plasmas have been shown to alter the deposited thin film thicknesses and increase selectivity in etching, as well as introduce new chemistry and reduce charge accumulation. As a result, they have been investigated for use with plasma thrusters, atmospheric glow discharges, inductively coupled plasmas, and capacitively coupled plasmas. Capacitively coupled plasmas currently have very limited use in industry due to mismatch problems with the matching network. These problems arise from how the plasma is formed, leading to variations in power received by the plasma. This paper will detail the beginnings of a project whose ultimate goal is to create a feed-forward, feed-backward control to non-invasively characterize the plasma in real time, and appropriately alter the power of the generator to alleviate the problems with matching network.

This characterization was performed using two generators that deliver power to one electrode, while the other electrode was floating. One generator was pulsing while the other remained on, to mirror industryâĂŹs use of multiple generators and to always have a signal to measure on the VI probe. The VI probe used in this experiment is capable of taking measurements on a microsecond time scale. With this equipment set-up, the transients of the plasma were characterized.

The impedance measurements from the VI probe were used to examine the changes in sheath thickness over a pulse cycle. Looking at the transient region where the pulsing generator turned on, four regions were clearly evident: the background sheath when the pulsing generator was off, the change in electron temperature, the change in electron density, and the background sheath when the pulsing generator was on. Plasma parameters were adjusted to study their effect on these regions. Pulse frequency was increased and with that was seen an increase in electron temperature. This was caused by the electrons having less time to diffuse and thus more being present at the beginning of the next pulse cycle. Resulting in the plasma having more time to spend heating the electrons rather than creating new ones.

The power both generators were exporting was varied independently. The generator operating at a constant power saw a drop in sheath thickness with increased power while

the pulsing generator saw an increase in sheath thickness with increased power. This was due to the frequency of the generator, depending on generator frequency either the power will be deposited into the bulk or into the sheath. Lastly argon and oxygen were mixed at different partial pressures. A difference in electron density was identified which was independent of pressure, but varied with increasing oxygen. These differences are believed to be the result of the vibrational state of oxygen creating low energy electrons.

Time resolved hairpin probe measurements need to be taken to fully characterize the changes in the transient regions with respect to plasma conditions. These measurements will complete the verification of a model that has already been created of a pulsed capacitively coupled plasma. After which, all of the data taken will be handed off to our industry partner to be used in the creation of a generator which can modulate power.

Investigation of the Transient Regions of Multi-Source Pulsed
RF Capacitively Coupled Plasma Discharges

by
Theresa Kummerer

A thesis submitted to the Graduate Faculty of
North Carolina State University
in partial fulfillment of the
requirements for the Degree of
Master of Science

Nuclear Engineering

Raleigh, North Carolina

2015

APPROVED BY:

_____   _____
Mohamed Bourham   Jerome Cuomo

_____
Steven Shannon
Chair of Advisory Committee

DEDICATION

To Ms. Weaver, my first grade teacher, for teaching us to be engineers all those years ago in and out of class. You fanned the flame for scientific inquiry.

BIOGRAPHY

The author was born, did a bit of living, then wrote the following.…

ACKNOWLEDGEMENTS

TABLE OF CONTENTS

LIST OF TABLES

LIST OF FIGURES

CHAPTER

1

INTRODUCTION

1.1 What is a plasma, how is it formed?

Matter. Every object is made of it. It comes in different size, shapes, and consistencies. The molecules or atoms making up solids are tight packed and make up a regular pattern. When energy is added to this system, the molecules or atoms begin to move about losing their regular pattern and becoming more spread out. The more energy, the faster the molecules or atoms will move until a gas is created. Adding more energy to a gas will cause the electrons in the atoms to excite which will create light. If enough energy is applied electrons are liberated from their atom creating a plasma.

Radiant matter (plasma) was first studied in a laboratory setting by Sir William Crookes in 1879[10]. It took science some time to be able to characterize and understand what plasma is. With J.J. Thompson's discovery of the electron in 1897 the nature of plasma was first identified[46]. 1928 was when the fourth state of matter was formally named plasma, for how the entirety of the matter reacts to being acted upon at one location, like in blood plasma[24].

While plasma is the state of matter most often forgotten it is everywhere and makes up

the vast majority of all baryonic mater. The sun and every star in the sky are composed of plasma. Down on Earth, it is most commonly found in lightning, lasers, and fluorescent lights; plasma is used to make nonstick pans and the semiconductors in electronics and to sterilize medical equipment. Some more examples of plasmas are shown in Fig. 1.1 plotted in correspondence with their respective electron temperature and electron density ranges.
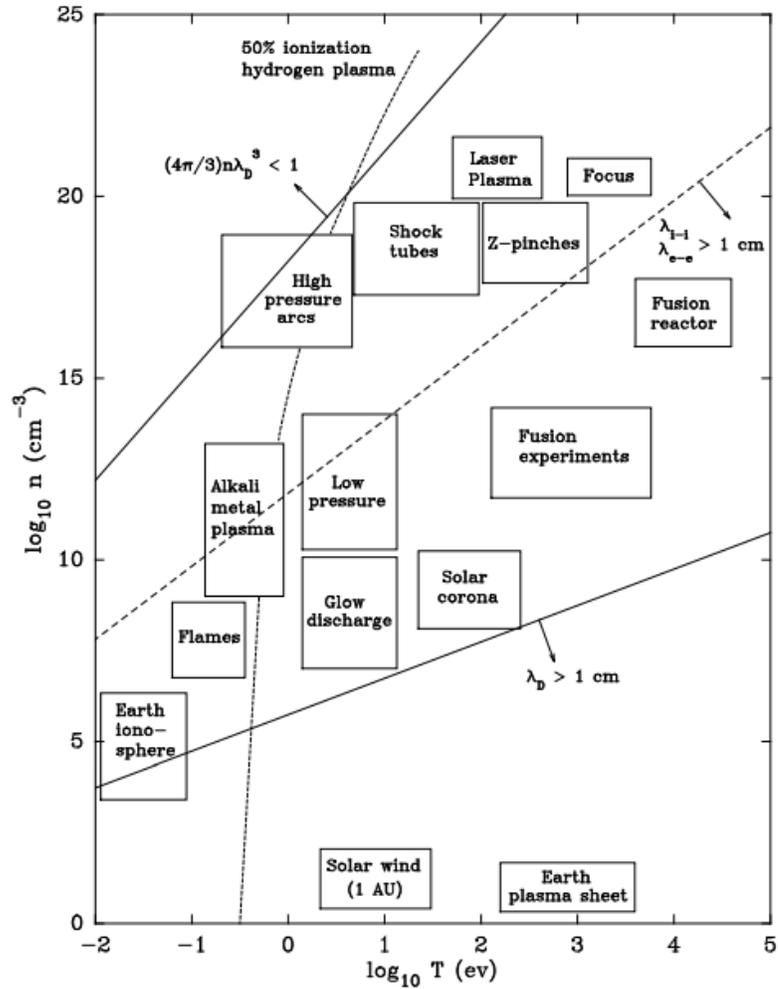
Figure 1.1: Types of plasmas[17]

1.2 Power supplies

DC can operate without a matching network and uses a cheaper generator than RF. DC powered plasmas are used for sputtering, in accelerators, and plasma speakers. DC is limited because it cannot operate with insulators nor with all plasma antenna configurations. RF can also be used for sputtering and offers a greater sputtering depth than DC, though DC is still preferred in some cases because of cost.

Accelerators are comprised of an entrance injector for ions. The ions are then accelerated through a series of rings of ever increasing voltage, as seen in Fig. 1.2. Once the power is turned on the ions begin to accelerate. RF discharges supply time varying periodically oscillating power. Using DC provides a continuous beam of ions, if RF was used the ion supply would be pulsed.
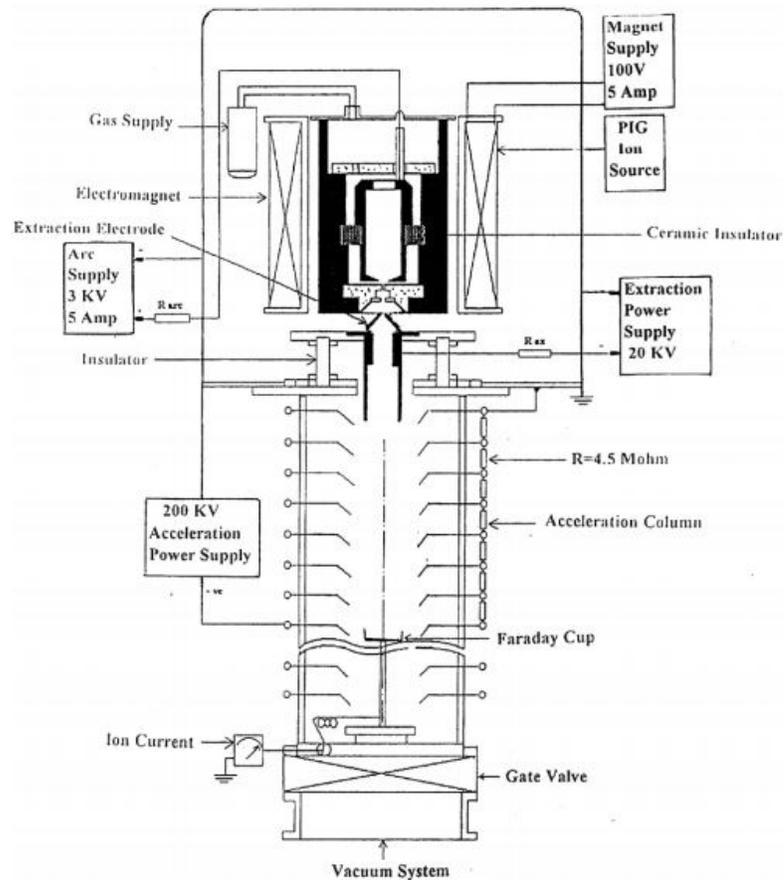
Figure 1.2: Plasma accelerator diagram[34]

RF discharges are broken up into sub groups depending on the frequency at which they operate in and their power coupling mechanisms. The group divisions are fuzzy and continue to change as technology improves. This project used high frequency (HF), which starts at about 100 kHz and goes to about 13.56 MHz and very high frequency (VHF), which stretches from about 27 MHz to 162 MHz.

1.3 Antenna Configuration

Just as there are many power sources, there are also many ways to create a plasma. This document will focus on inductively coupled plasmas (ICP) and capacitively coupled plasmas (CCP). There are several books currently in print that discuss the equations that govern inductive and capacitvely coupled plasmas, I suggest Principles of Plasma Discharges and Materials Processing[26]. Instead of giving a summary of those equations this paper will focus on how each is used in industry by discussing the pro et contra of each discharge.

1.3.1 Inductively Coupled Plasmas

An inductively coupled plasma (ICP) is made up of a coil of wire with an electric current flowing through it placed near a vacuum chamber. The wire can be wrapped around the chamber; this is common for research reactors in that it ensures a large plasma with uniform properties. Or, the wire can be wrapped to be a 2D coil similar to the heating coils for stoves. ICPs are used in many applications for example mass spectroscopy, and etching.

Mass spectroscopy works by ionizing a compound for the purpose of determining the chemical composition of the compound. The electrons are magnetically sifted, out so the ions can be accelerated alone, through an arc by more magnets to a target. The lighter the ion the more it will curve, enabling the target to extrapolate the atomic mass based on position of impact. The relative abundances of the ions are then used to determine the chemical make-up of the compound.

Ionization of the compound is achieved by interaction with an argon plasma created by an inductive source. Argon is used because it has a high first ionization energy[1], meaning when it impacts with the sample compound it will have enough energy to ionize the compound. While not being so high as to cause secondary ionization of most compounds, this would not be a bad thing it would simply be unnecessary. ICPs are primarily used in mass spectrometers. Mass spectroscopy is conducted on solids, liquids, and gasses; ICPs operate

in a wide range of pressures so a compound changing state wonâĂŹt extinguish the plasma. ICPs control ion flux independently of other plasma parameters, a mostly ionized plasma is needed to make the most of plasma-compound collisions, consequently ICPs are ideal for this in that the user can have a highly ionized plasma without sacrificing anything.

The electrodes used in ICPs can be located outside of the chamber, keeping them from becoming degraded over time due to the gases introduced to the chamber and processes occurring within it. ICPs are ideal for etching because they create non-uniform plasmas. A uniform plasma would etch faster in the center than at the sides as seen in Fig. 1.3.1. The center of the wafer, B, would be acted upon from straight above and from the sides, while at the edge of the wafer, A, the plasma would only be acting from above and one side. Ion acceleration occurs only in the sheath, so if a sheath is thinner at the center even though the wafer will be acted upon by more ions there this can be canceled out by the ions traveling slower thus individual ions have less of an effect, making etching uniform across the wafer. If the ICP is etching a wafer unevenly, this problem can be more easily fixed than with a CCP. With ICPs being coils, it is easy to introduce another coil to modify the topology of the plasma.
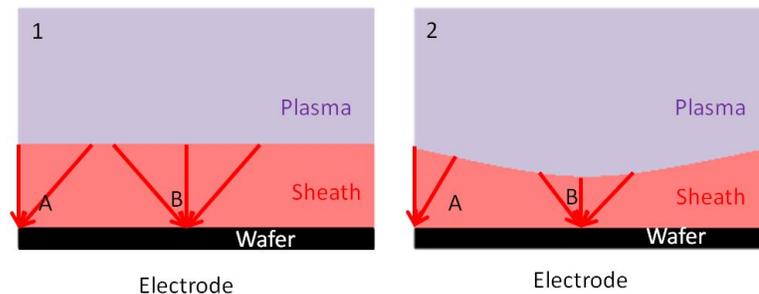
Figure 1.3:   1. A uniform plasma, the center, B, is being acted upon from more directions than at A. 2. A nonuniform plasma, while the center is still being acted upon from more directions the ions are not being accelerated as fast as at the edge.

Unfortunately ICPs can only be powered by RF. DC cannot sustain the plasma and any RF frequency higher than 13.56MHz runs into issues with Ohmic heating. In addition there are oscillations present in ICPs because inductive sources are active in a capacitive mode[26]. This is necessary because the magnetic field created by the coils is not sufficient to create a plasma. Via alignment of the coils and positioning of a Faraday cage the electric

field can be minimized or be done away with. If the electric field is removed, then additional equipment is necessary to strike the plasma.

1.3.2 Capacitively Coupled Plasmas

Capacitively coupled plasmas (CCP) are created by flowing electricity between 2 parallel metal plates with a gas present between them. CCPs are used for plasma-immersion ion implantation, and deposition.

Plasma-immersion ion implantation is a recent development in the ion implantation industry. Ion implantation was first investigated in 1911 by Rutherford and his students, patented in 1949. Ion implantation was first used to dope semiconductors to create pn junctions. In the mid-seventies it started being used to surface treat metals. Doping a metal with nitrogen or carbon could increase the metalâĂŹs resistance to corrosion or wear. With metal came the want to treat three dimensional objects, and issues with size and uniformity. This led to work with arcs which lead to plasma-immersion ion implantation. Plasma-immersion ion implantation has shown the ability to alter the physical and chemical properties of not only semiconductors and metals but also of polymers, plastics, glass, and ceramics[15].

CCPs are used for deposition because they offer uniformity, this is created by the stabilization of the sheath caused by the difference in sheath and plasma impedance[14], making CCPs the choice antenna for thin film transistors and other large area applications[6].

For deposition and etching, chemistry is frequently investigated as a means for improving the process. Argon-hydrogen discharges are frequently chosen for sputtering deposition leading Neyts Yan, Bogaerts, and Gijbels to model the electron energy probability function and electron density for varying hydrogen partial pressures. She discovered that hydrogenâĂŹs vibrational state causes a distribution in electron energy where by the electrons were split into a fast and slow group. The increased quantity of low energy electrons results in electrons becoming trapped in the plasma at small hydrogen partial pressure causing an increase in electron density. As hydrogenâĂŹs partial pressure is increased, there is a greater number of high energy electrons possessing enough energy to escape the plasma and be lost to the walls. This results in a drop in electron density as seen in Fig. 1.4[11]. This phenomenon is investigated in this paper to see if it can be repeated for an oxygen pulsed plasma.
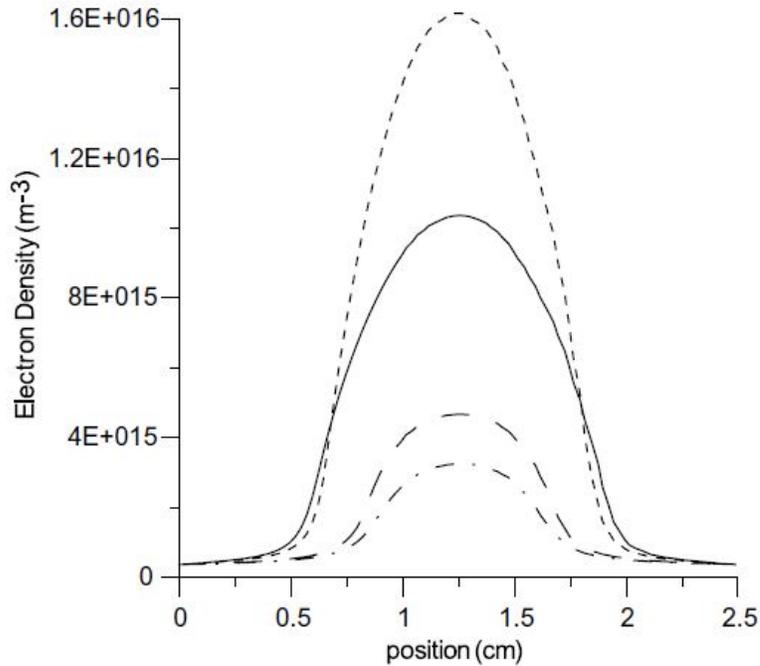
Figure 1.4:   Calculated time-averaged electron densities for argon (solid line), 1% hydrogen (dashed line), 5% hydrogen (large dashes), 10% hydrogen (dash dot line).[11]

1.4   Pulsed Plasmas

Pulsed plasmas have shown tremendous promise for extending plasma processing. For example reducing damage to the processing sample; specifically in terms of charge build up, and dust particle formation which results from the trapping of negative ions in the plasma[49, 4, 8]. Ankudinov, Bobashev, and Andreev showed that thin film thickness can be increased by altering duty cycle and that the quality of the film could be improved[49]. Furthermore, pulsed plasmas introduce new chemistry which are prohibited in CW plasmas; for example, the density of fluorocarbon radicals can be manipulated, which in turn can increase the selectivity of the etching processes[36, 16, 23], as seen in Fig. 1.5. In addition pulsed plasmas have been shown to reduce etching anomalies[37, 28, 38, 42] as seen in Fig. 1.6. The plasma in CW mode created notches at the bottom of the etch whereas the same plasma pulsed has much straighter lines. Pulsing has also been shown to have the same etch rate as CW while operating at a lower power[7].

Due to the numerous benefits offered by pulsing, pulsed plasmas have been investigated with a multitude of antenna configurations for use in several different applications, such as

7
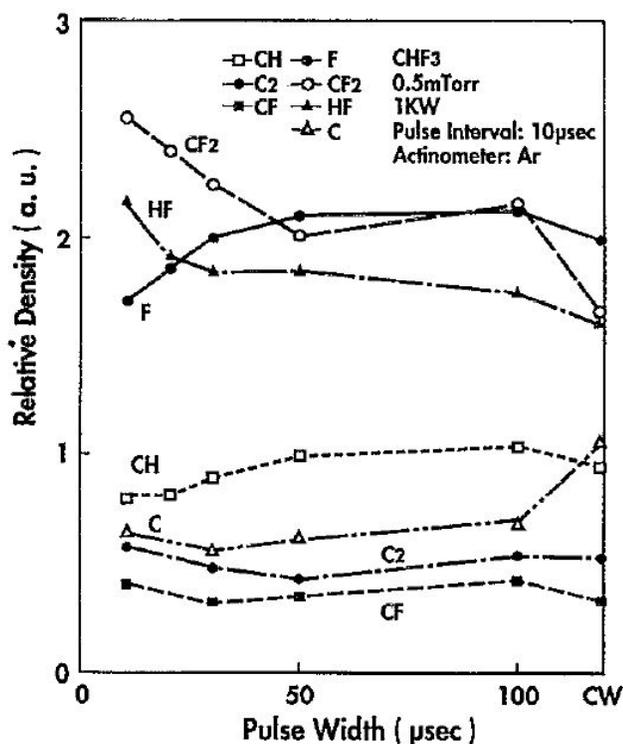
Figure 1.5: "Trends of relative density for CF_2, F, C, CF, CH, C_2, and HF, in CHF_3 plasma on pulse width."[36]

for thrusters for satellites. Thruster designs are typically coaxial, in that there is a center, cylindrical electrode within a metal tube. The tube acts as the cathode and the center wire the anode. Ziemer, Cubbin, and Choueiri showed that pulsing will achieve a high impulse and efficiency using low power[21]. Most of the thruster work investigated detailed changes in geometry and dimensions of the electrodes and the subsequent effect on the plasma. Ziemer, Choueiri, and Birx went on to investigate changing the capacitance and determined that increasing the capacitance caused an increase in thrust[20]. Keidar, Boyd, and Beilis showed that by introducing Teflon to the electrodes, the plasma density and subsequently acceleration could be increased. The plasma was hot enough to decompose the Teflon causing the Teflon to become part of the plasma[27].

Pulsing has also been investigated for atmospheric pressure glow discharges. Dielectric barrier discharges, the most common atmospheric pressure glow discharge, resembles a capacitive discharges; however, there is a dielectric material present between the electrodes.

8
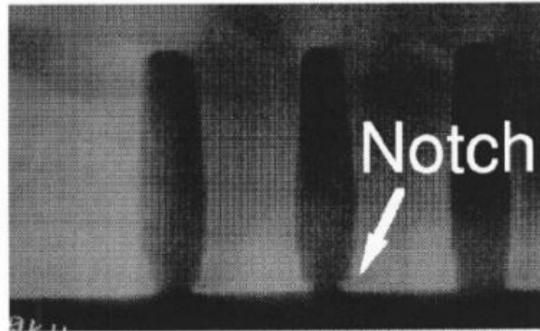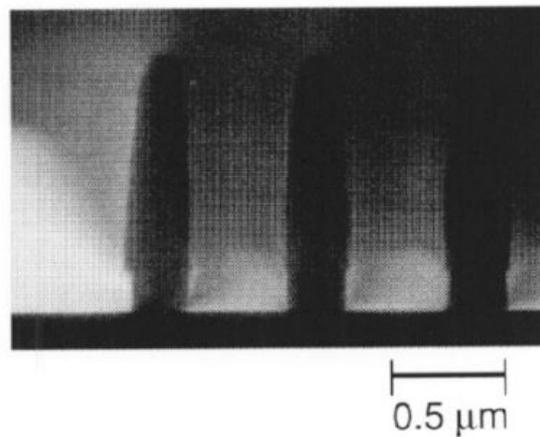
Figure 1.6:   "Cross sectional SEM photograph of the gate poly-Si etch in (a) CW mode and (b) pulsed-power mode...."[42]

Atmospheric pressure glow discharges operate at higher temperatures and consume more power than dielectric barrier discharges. Pulsing has shown the ability to decrease the temperature, because the off cycle allows the electrons to diffuse to the electrodes, and thus will not be present in the next pulse cycle. Electrons present at the beginning of the pulse act as seeds for the plasma causing the plasma to strike faster as it doesnâĂŹt need to build up as many electrons. Shi et. al. investigated this phenomenon and determined at what point the electrons had diffused enough to lower the plasma temperature[19].

Tests done in vacuum chambers tend to focus on finding solutions to a problem or improving current methods (selectivity in etching or understanding how pulsing is changing the plasma), rather than changing the geometry to optimize the plasma, as with thrusters.

The effects pulsing has on chemistry has been extensively studied as a means of improving etching processes. Etching of silicon dioxide is typically done with fluorocarbons. $CHF_3 \rightarrow CF_2 + HF$ is a low energy endothermic reaction, while the formation of CHF_2, CF_3, CF are highly endothermic reactions. All of these reactions happen simultaneously in a CW plasma, and one of the highly endothermic reactions uses the low endothermic reaction product, CF_2, as a reactant. Pulsing reduces the energy available, limiting the production of high energy products, while allowing the less energy intensive CF_2 to be maintained in higher amounts as seen in Fig. 1.5[36]. It has been shown that etch selectivity is increased, producing cleaner etches, with short pulse on times and longer pulse off times[16], demonstrating that low energy reactions are more selective in their etching.

Etching is done with and without plasmas and creates some nasty byproducts such as CF_4 which is a known greenhouse gas. Fortunately, plasma can be used to decompose CF_4. Kuroki, Tanaka, Okubo, and Yamamoto investigated if pulsing the plasma might alter the chemistry of the end products. He showed that pulsing could obtain the same level of decomposition and that pulsing modified the relation of the end products, producing more COF_2 and less CO. COF_2 can be easily removed with a chemical scrubber, whereas CO is toxic to humans[47].

Pulsing has also been investigated to improve deposition of thin films. By varying pulse frequency, the electron density has been shown to both increase and decrease relative to a CW plasma. The increase in electron density results in a subsequent increase in film thickness as seen in FIG. 1.7[30]. This phenomenon was further investigated via manipulating of duty cycle, using the frequency that Overzet and Verdeyen found to maximize sheath thickness. It was found that increasing duty cycle resulted in a slower deposition rate. However, since the plasma was on longer, a duty cycle of 60% actually had the largest thickness. This effect occurred as Si, SiH, SiH_2, the other molecules responsible for the creation of thin films, have a short lifetime and decay away quickly at the end of each pulse cycle. Allowing SiH_3, which has a longer lifetime, to have a greater presence in the film. SiH_3 is not a radical like SiH_n (n=0-2), thereby increasing its presence in the film increases the quality of the film[49].

CCPs have lagged behind ICPs on the scientific expedition for discovery. CCPs have been extensively modeled [31, 44, 40]; however, it took sixteen years since the time the first one of those papers was published for someone to acquire the experimental data to verify the findings. The study used both a Langmuir probe and a RF current sensor. Both of these diagnostic tools were placed within the chamber; thus both perturbed the plasma in taking
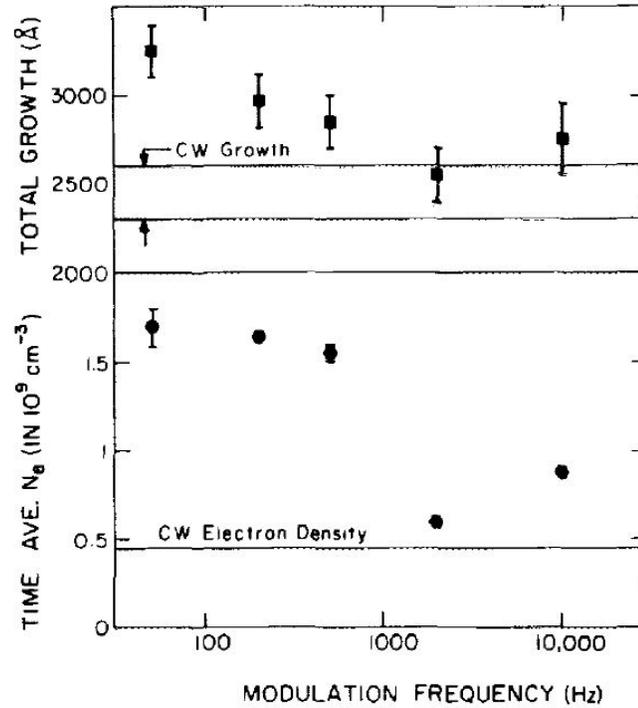
Figure 1.7: "Total film thickness after 15 min and time averaged electron density during the growth as a function of the modulation frequency."[30]

data. Also, while this experiment was able to characterize trends with frequency, pressure, and power for both generators it was operating with, thus verifying theoretical results, none of the data was taken with respect to time[12]. Leaving a gap in our knowledge of what is happening in a CCP discharge.

There have been other studies done with CCP discharges that do take time resolved data [45, 22]. But there is still a gap in our knowledge as to how exactly the plasma reacts immediately after power is turned on or off. It is known that when a pulsing generator changes power it causes all the other generators to that are not perfectly matched to become mismatched, causing the plasma to fluctuate. Fig. 1.8 shows the Smith Chart trajectory of a generator run in CW mode while another was pulsed. While most of the time is spent with less than 20% of the power being reflected, the center 2 x 2 box, the majority of the time is spent with more than 10% of the power being reflected.

The automatic tuning capabilities of the matching network cannot be used to find a best match position because the pulse cycle is faster than the tuning capabilities of any matching network. Also the best match for generators running in CW will not be in that
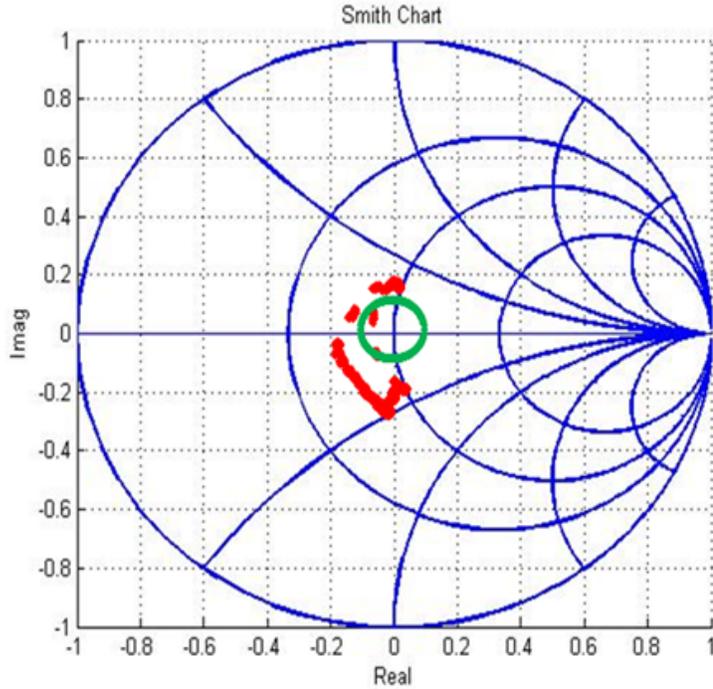
Figure 1.8: The red line is the match of the 13MHz generator while the 27MHz was pulsing for a 200mT O_2 plasma. The green circle is 10% reflected power.

same position for pulsing[29], so this problem cannot be easily worked around. Currently the only way developed to combat this is to use high precision capacitors, Fig. 1.9. Fig. 1.9 shows the power delivered from a generator in CW mode. There is a second generator that is pulsing which causes the fluxuations in the power. Both generators are being used to create an argon plasma, this model is based off the transients seen in [41]. The red line models V_{DC} compensation, assuming all the power goes to the plasma. The blue line models V_{DC} compensation plus mismatch. Unfortunately, this fix must be highly precise; a change of 10pF can be enough to cause issues as seen in Fig. 1.9. As a result of match variability and chamber matching, this is not a feasible solution for industrial applications. Currently this problem is avoided by passively matching RF power delivery, synchronize power supplies, and limiting operating conditions. This limits the uses of pulsed CCPs, making pulsed CCPs viable for only a small number of industrial applications.

Power fluctuation is also a problem for ICPs, as ICPs have a high Q circuit, making it very easy to fall out of inductive mode. Overall, CCPs are not harder to work with; they simply haven't been investigated as thoroughly.
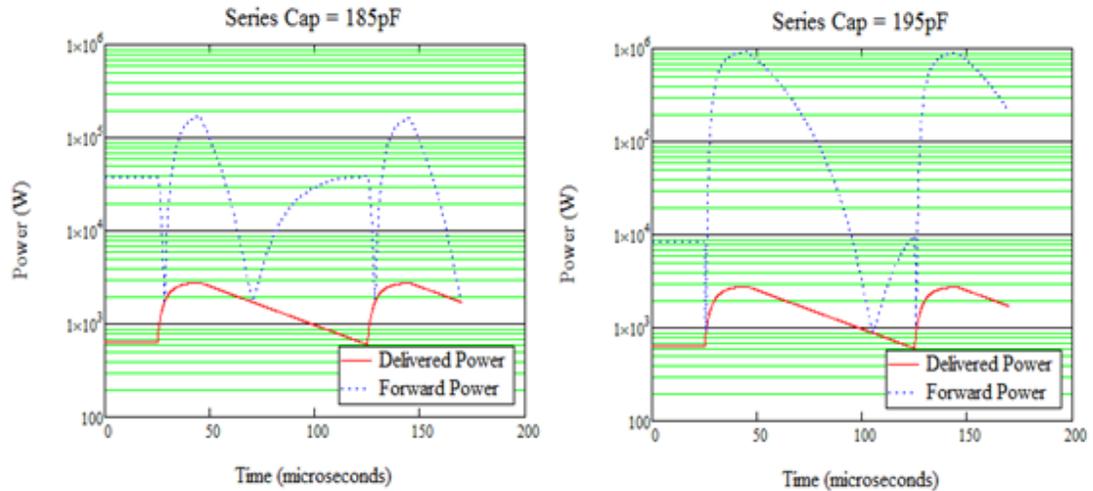
Figure 1.9: Left shows a forward power supply that is fairly uniform between pulses with respect to both height and width. Right shows the same conditions with the addition of 10pF to the matching network, the forward power supply now shows no uniformity between pulses. Photo courtesy of Steven Shannon.

It is the goal of this project on creating a feed-forward, feed-backward system using frequency tuning to modify the power coming out of the generators, thereby eliminating the matching network problems while not being a one chamber solution. This paper details the initial data collection phase of the project, where the transient regions of the plasma were characterized.

1.5 Thesis Layout

The equipment used in this experiment is outlined in chapter two. The chapter begins with a description of the chamber and power delivery system. It then moves on to describing the electrodes and the water cooling system devised to keep them from overheating. Next the chapter discusses the equipment that was investigated to characterize the plasma.

Chapter three details and discusses the findings of the experiment. First explaining the math and assumptions used to analyze the data, and then focusing on the transient regions of the plasma, explaining the changes in slope seen there. Initial conditions are then modified to determine the effect on each region as part of a background study.

Chapter four ties everything together. It concludes and summarizes the work done in

this experiment. This paper ends with a discussion on future work that should be done.

CHAPTER

2

EXPERIMENTAL APPARATUS

Chapter 1 introduced the discovery and description of a plasma, then dove deeper into the type of equipment that can be used to make a plasma. Specifically, RF and DC discharges, then moved to the electrode configurations, focusing on ICPs and CCPs. A description of previous work on pulsed plasmas was then investigated, followed up with support for an investigation into pulsed CCPs. In this chapter the experimental apparatus will be described. Specifically discussing the equipment used to power the plasma, the chamber as well as the electrodes, and the equipment used to measure plasma phenomenon.

2.1 Chamber Design

The experimental apparatus used in this experiment is comprised of a parallel plate electrode encased in a vacuum chamber. The vacuum chamber is capable of regulating up to four gases at constant pressure. Plasma is struck by applying either pulsed or constant RF power to one or both electrodes.

The chamber used in these experiments is the NCSU's Modular Radiofrequency Plasma Chamber (MRPC). The MPRC is constructed out of stainless steel and is capable of holding

approximately 30 liters of gas at atmospheric pressure. Oxygen and/or argon were used in this experiment. The plasma is formed between two parallel 6 inch diameter electrodes designed for high efficiency RF coupling from the kHz range to 200 MHz. All of the power was delivered through one electrode, the other electrode was floating. More details on the electrode design are available in section 2.2.

In this experiment power was delivered from a MKS LVG3527A generator to a home built dual frequency matching network and from an ENI GHW-50A Gensis RF model generator to a RF Power Products Inc. AM-10 matching network. The MKS generator ran in slave mode to a Agilent 33220A waveform generator so that it could be pulsed, as seen in Fig. 2.1, pulsing was done between some set power and zero. The MKS generator pulses using a switch rather than an amplifier. Both can pulse at very high frequencies; however, amplifiers can offer better isolation[3]. The ENI generator was used to send out a signal in constant waveform (CW) mode.

Matching networks are used to minimize power reflected back to the generator caused by transmission mismatch. The home built matching network was designed to work as a match for the MKS generator, as well as to combine that matched signal with the output from another matching network and output both from a single point. This unique feature was needed as the chamber was designed to only receive one input per electrode. In a previous experiment, one generator was connected to each electrode but a plasma could not be struck reliably and when produced, it could never be matched well.

Generators are guaranteed to work within a couple hundred hertz of the frequency they are marketed at. This nearly guarantees there will be some difference in the pulses produced from harmonic generators unless they are phase locked, which was not done in this experiment. Fig. 2.2 shows the amplitude of combined waves with frequencies of a 13.56 MHz and 27.12 MHz, where the red line is when the two are perfectly in phase and the blue line is when there is a difference of 400 Hz between the two. Demonstrating that a small difference in two harmonic frequencies will cause the intensity of the plasma to oscillate, in what is called a beat frequency. The generator frequency was modulated slightly from 13.56 MHz and 27.12 MHz to produce frequencies at 12.88 MHz and 28.476 MHz, respectively. By modifying the frequencies to be as far away from harmonics as possible the problem is remedied. The combined waveform still changes over time but the change is now longer than a pulse cycles.

The base pressure of the MRPC is 0.1 mTorr with a leak up rate of 3.4 mTorr/minute. Pressure was monitored and controlled via a MKS baratron (0.1 mTorr - 1 Torr). The baratron
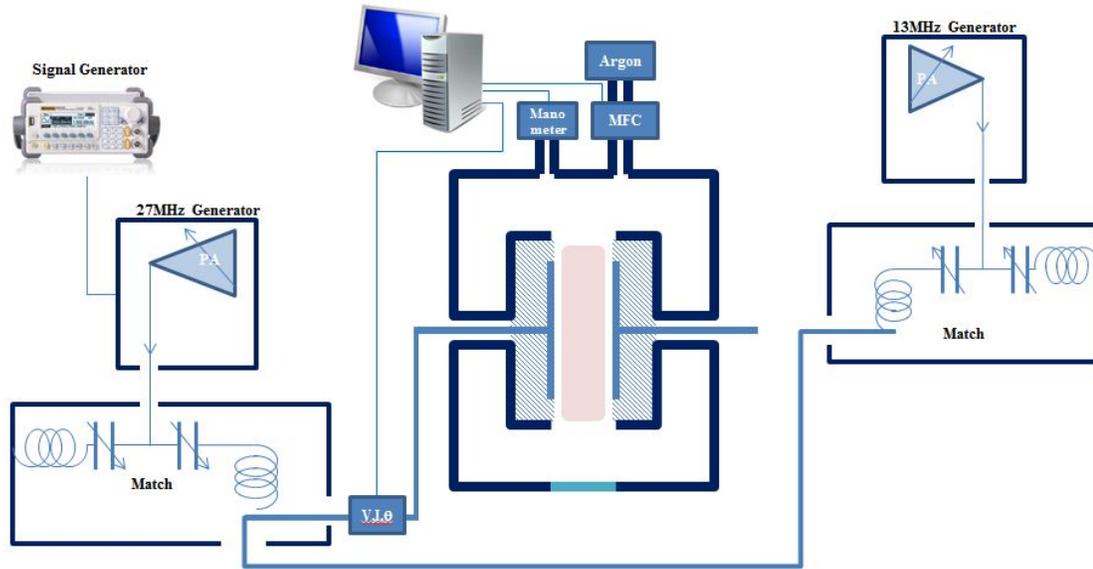
Figure 2.1: Detailed experimental setup for power delivery. The counter electrode is terminated through rexolite, coupled to ground through a 2.5 ft RFG transmission line.

sends this data to a MKS pressure controller which adjusts a throttle valve to the desired pressure. Mass flow controllers were used to adjust the amount of gas being sent from the gas tank to the chamber.

Measurements were taken using a MKS VI probe, a National Instruments Pi-Max 3 camera, an Impedance Langmuir probe, and a hairpin probe. The VI probe was placed between the last matching network and the chamber. The camera was aligned perpendicular to the electrodes, looking into the bulk of the plasma. The Langmuir probe and hairpin probe were placed, one at a time, between the electrodes slightly off center in favor of the floating electrode.

2.2   Electrode Design

The electrodes are held in place by a pair of 1.25 inch wide tubes that extend through an Ultratorr fitting to outside the chamber. This is seen as the tube connecting the VI probe to the capacitor on the left of Fig. 2.4 and back out on the right from the capacitor to nothing. This allows for the gap between the electrodes to be adjusted from 1/2 an inch to 3 inches. The gap was kept constant at 3/4 inch for all experiments.
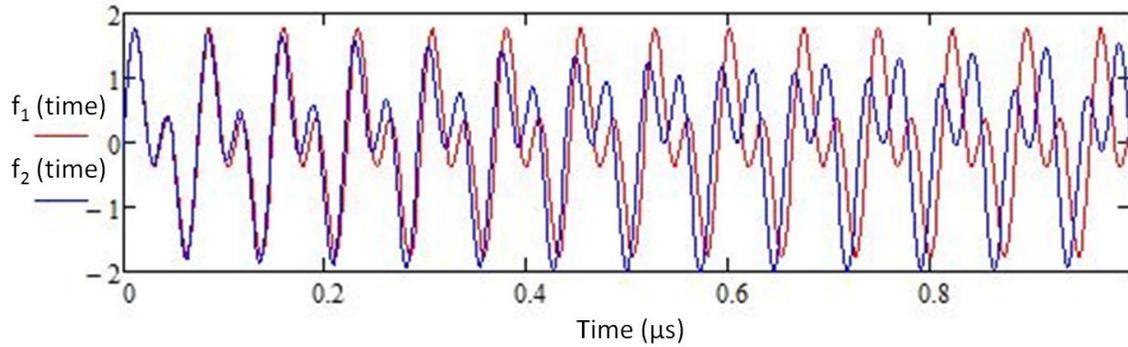
Figure 2.2: f_1 is the combination of the 13.56 and 27.12 waves f_2 is the same with an additional 0.4, t is time.

The tube is welded to a flat plate in order to provide a connection to the bucket housing the electrode inside the chamber. There are 6 holes in the bottom in the plate; the center hole is surrounded by five 5/16 inch holes evenly spaced a distance 4 inches from the center. The aluminum bucket, which acts as a grounding shield, is connected to the flat plate by five ultem bolts. As seen in Fig. 2.5 the aluminum bucket holds a rexolite bucket, which holds two aluminum plates. The rexolite is used to isolate the plates so they will not be grounded. As noted in each of the pictures an O-ring is present between each layer. This provides an air tight seal between the layers, as the power supply side is at atmosphere. There is an O-ring between the two aluminum plates Fig. 2.5(B) that was excluded from this picture for clarity in that small space. The center hole is occupied by a N-type bulkhead coaxial connector. The system is supplied power via a low insertion loss coaxial cable which is fed through the 1.25 inch diameter pipe.

2.2.1   Water Cooling

In the course of running experiments, the bolts on the powered electrode sheared. This was due to the metal electrodes heating up and expanding faster than the ultem bolts; straining them until failure. This was the second time this had happened to the MRPC so a system to cool the electrodes, preventing the bolts from failing again was created. The chamber is kept at 0.1 mTorr when not running experiments and while experiments are being run doesn't tend to be run above 400 mTorr preventing convective energy loss from efficiently cooling the plates. The rexolite used to isolate the electrodes, so they would be floating, also acts to thermally insulate the electrodes, preventing much conductive heat loss. It
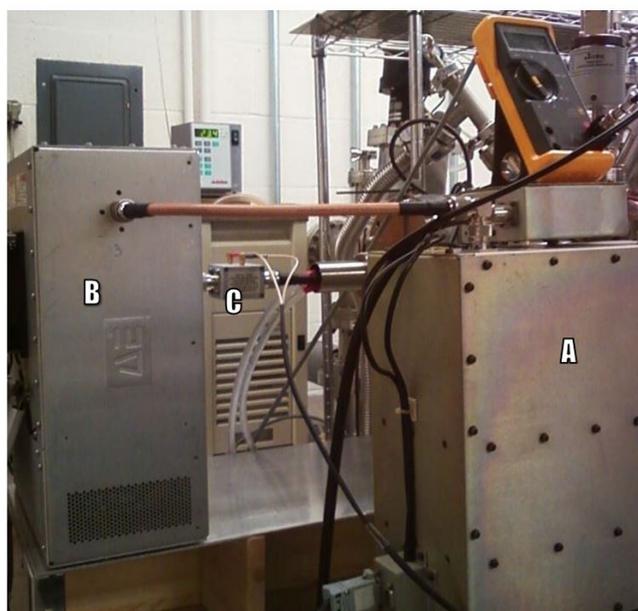
Figure 2.3: A is the 12.88 MHz match running into, B, the 28.476 MHz match. C, is the VI probe, located between B and the chamber.

was determined that the only way to sufficiently cool the electrodes without dramatically changing the pressure or limiting the duration experiments could be run for, was to water cool the electrodes.

One channel of water flowing through the electrodes was calculated to be sufficient. As noted in Fig. 2.5, the electrodes are actually two aluminum plates, allowing a channel to be carved in the back of one plate. The bolts hold the plates together enabling the water to cool the center of the electrode, while minimally changing the existing electrode design. The channel was carved out in a flower like pattern to ensure that the electrode would be cooled semi-evenly while maximizing the available surface area, as seen in Fig. 2.6.

Custom made rexolite connectors were constructed to connect the channel to the tubing. Rexolite was chosen for its high electrical insulation and high decomposition temperature. The custom design was necessary due to the limited space available to make the connection, since this to had to go through the 1.25 inch diameter pipe, and no commercially available product could fit the space. The liquid used to cool the electrodes is deionized water, run in a continuous loop from pump and chiller to electrodes to water polisher and back to pump. The water polisher is used to deionize the water thus removing any contaminates or charged particles in the water, keeping the water from grounding the electrodes.

The water cooling system dispenses 300mL of water to each electrode every minute. In
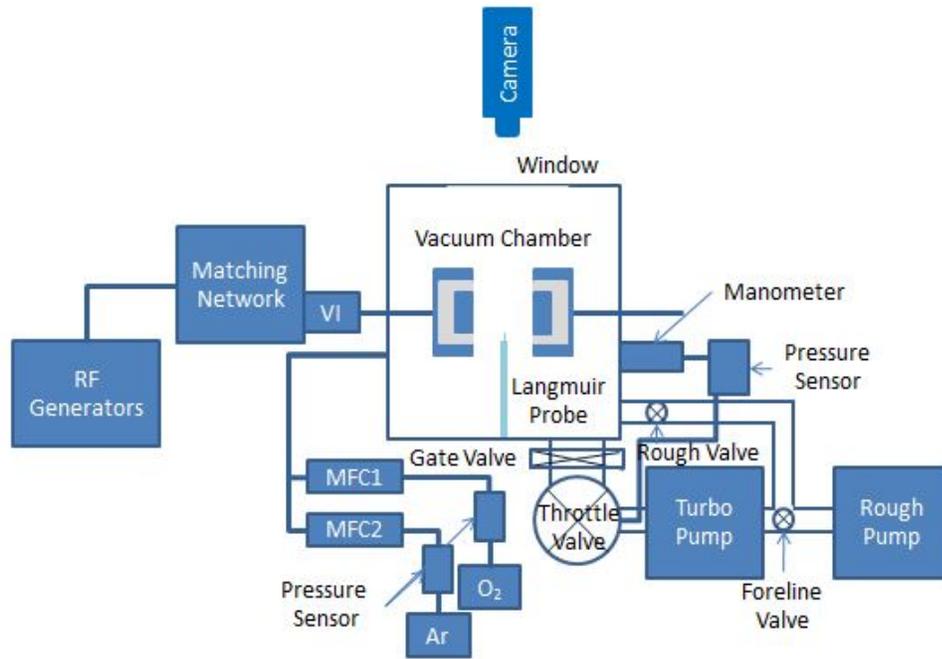
Figure 2.4: Detailed experimental setup.

a test of the effectivity of the cooling system, a plasma was ignited for 10 minutes then the chamber was returned to atmospheric pressure and the temperature drop was measured over a 10 minute period as a control. This was then repeated, except at the end of the second plasma run the water cooling system was also turned on. The chamber had to be returned to atmospheric pressure because our lab only has an IR beam thermometer for taking temperature and the beam cannot penetrate the quartz window of the chamber. It was determined that the water cooled electrodes cooled at 0.873^0C/min, a rate that was 85% faster than stagnant room temperature air alone, ensuring that the system wouldn't fail fail to heat, so long as water was run through the electrodes at all times. Before this system was put in place the electrodes needed to be replaced after about 20 RF hours. Since implementing the water cooling system the chamber has been run for 60 RF hours at comparable power without issue. While this system is quite effective at keeping the electrodes cool, it does nothing for the grounded shield. In the future it may become necessary to design a water jacket to keep the grounded shield cool as well.
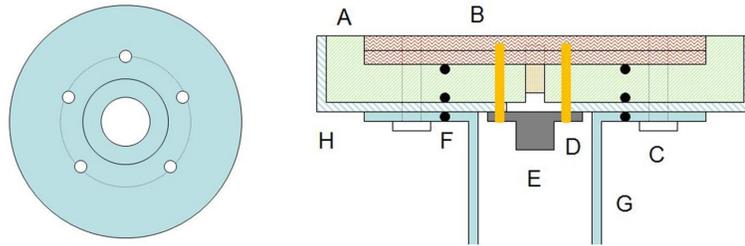
Figure 2.5:   The left shows the hole layout, while the right is side cut of the electrode setup. A: Rexolite B: Stainless steel plates C: Ultem bolts D: (Yellow line) Water line E: Bulkhead connector for co-axial cable F: (Black circle) O-rings G: Stainless steel tubing H: Stainless steel bucket

Figure 2.6:   The center shows the flower patterned water channel surrounded by an O-ring and the holes for the bolts to hold it all together.

2.3   Plasma Diagnostics

In this experiment a variety of diagnostic tools were enlisted to characterize the plasma.

2.3.1   Optical Emission Spectroscopy (OES)

To measure changes in the sheath thickness with respect to time, an attempt was made to use optical emission spectroscopy. This was performed using a Pi-Max 3 1024i camera to take the pictures. The camera takes images in the optical spectrum with a resolution of 1024 x 1024 pixels and has a frame rate of 32 MHz. The camera was aligned to see straight between the electrodes, as seen in Fig. 2.4, and WinSpec, a program made by Princeton Instruments, was used to control the camera. WinSpec set the shutter speed, adjusted

the resolution, and combined pictures, allowing for images to be taken with a fast shutter speed in low light. Pictures were taken on a 1 μs time scale, as it was impossible to take clear pictures any faster regardless of how camera settings were adjusted. The timing of the images was controlled using a waveform generator that was connected to both the 28.476 MHz pulsed generator and a BNC model 575 pulse/delay generator. The pulse generator was used as an external trigger for the camera, allowing for the photos to be taken at varying, known, points in the pulse cycle.

Each 2D picture of the plasma was simplified to a matrix of intensities enabling the information to be read and analyzed by programs other than WinSpec. The intensities were then compiled into a 1D line, and the second derivative of that line was taken as seen in Fig. 2.7b. The code used to construct Fig. 2.7 can be found in Appendix A. The thought being that the second derivative of the 1D line could be analyzed to find an inflection point which would be the location where the sheath began. The following algorithms were used to try and find this location: numerical differentiation, cross correlation, singular value decomposition, and simply using oneâĂŹs eyes. Unfortunately, none showed the sheath changing on the same time scale as the VI probe. Investigating argon, it was found that argon has several emission wavelengths that decay on the microsecond scale [32, 43, 9]. It is suggested that in the future, if OES is to be performed, that the gas used to create the plasma have a smaller atomic number, for example all of Hydrogen's emission wavelengths decay on a nanosecond time scale [48].

2.3.2   Voltage Current Probe

MKS's VI probe works in much the same way as other VI probes, measuring voltage, current, and the phase between then and calculating impedance from that, Fig. 2.8 shows a diagram of how that is done. Voltage to the plasma is determined by measuring the voltage drop across a capacitor. The capacitor is half a capacitor the other half being the hot cable. The probe is DC isolated which is why a resistor is not used to measure the voltage drop. Current is measured by measuring the time rate of change of magnetic field in the inductor, caused by changing current in the hot cable. The power runs through the air gap of the inductor, which is grounded on one side.

The MKS VI probe is comprised of three parts: a box that measures voltage and current, a box that process the measurements, and the cables that connect these boxes, ass seen in Fig. 2.9. All three parts are calibrated together and create a matched set. This is necessary
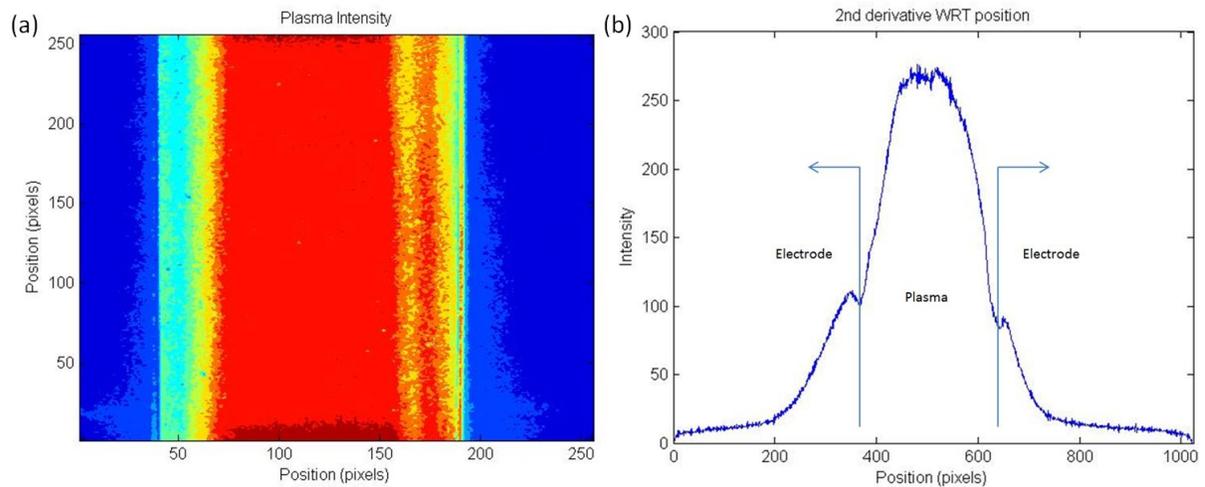
Figure 2.7:   (a) 2D plasma photo, each point represents 4 pixels. (b) 1D line of the intensities of (a). The first inflection point into the plasma from the electrode is the plasma-sheath border. The large bumps near the electrode edges are caused by the curved edge of the electrodes reflecting the plasma.

because unlike most probes, MKS' VI probe can take time resolved measurements on a microsecond scale. This is because the frequency sent out from a generator doesn't just stay at a point, it has harmonics, as seen in Fig. 2.10. The low frequency harmonics, while getting smaller with time also get closer together; consequently, at a frequency about double the initial frequency the harmonics are nearly on top of each other. As a result the more generators run, the more frequencies operated at, the harder it becomes not to include the harmonics in the desired measurement.
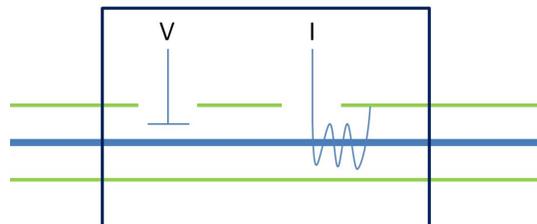
Figure 2.8:   The box is the VI probe interrupting the coaxial cable. On the right is an inductor used to measure current and on the left is resistor used to measure voltage. Both inductor and resistor are grounded to the outer shroud of the coaxial cable.

Figure 2.9:   Photo of entire MKS VI probe system[2].

MKS uses a narrow band filter to remedy this problem. Reviewing Fig. 2.11, the VI probe captures the voltage and current. The probe then parses out the data at the correct frequency, while breaking it down into its constituent sine and cosine wave form. This data is then down sampled because the probe is capable of taking data faster than the probe can process the data. The data then passes through a low pass filter to remove any noise after which the data is processed. Thus, the MKS probe is capable of producing data at a high sample rate, enabling us to take several measurements during the transient of the plasma.

Frequency is tracked by first programming the frequency synthesizer for the frequency of the RF source. It is noted that the MKS VI probe is capable of tracking up to 10 different frequencies. Because frequency can vary, the frequency synthesizer adjusts to maintain the position of the frequency. This is done by taking the derivative of the phase with respect to time.

$$ f = \frac{\delta \theta}{\delta t} \tag{2.1} $$

2.3.3   Langmuir Probe

The Langmuir probe was located between the electrodes, as seen in Fig. 2.4, slightly off center in favor of the floating electrode. The sheath on the powered electrode was larger thus
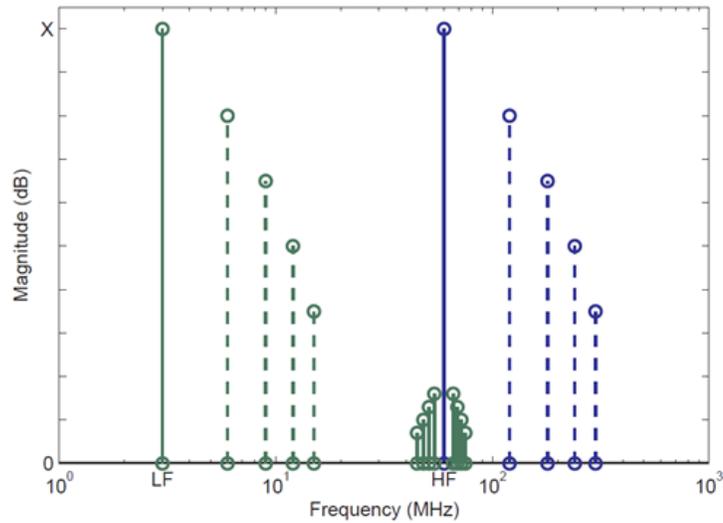
Figure 2.10: Harmonics of a low and high frequency pulse. Photo courtesy of Dave Coumou, MKS Instruments.

doing this kept the probe in the center of the plasma. The probe was used in advanced boxcar mode. This means, the probe was triggered by a BNC model 575 pulse/delay generator. The probe was set to sweep through a range of voltages for the entire transient period in 1 microsecond time steps. From this, it measures the floating voltage and calculates the electron density [18]. Unfortunately, the probe would visibly light up, meaning it was no longer measuring the plasma. Instead the probe would be measuring the light it was producing, this light was was caused by the voltage of the probe being too high compared to the plasma voltage making all data collected by the probe worthless. Despite decreasing the end voltage and time period data was only acquired while the probe was lit up or the voltage never became high enough to acquire any data.

2.3.4   Hair Pin Probe

Currently, we are working to develop a hairpin probe that will be capable of taking time resolved measurements. Typically, hairpin probes sweep through several frequencies to locate a point where the signal drops. Running the hairpin in boxcar mode, and keeping the signal fixed during the pulse; thus locating the point in time when the signal drops, will allow us to measure signal drop as a function of time, from that and Eq. 2.2[33] the electron

25
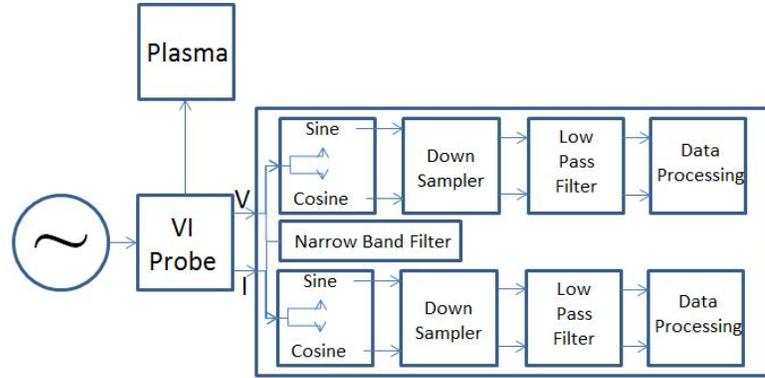
Figure 2.11: Diagram of MKS' VI probe components.

density can be determined as a function of time.

$$n/10^{16}m^{-3} = \frac{(f_r/GHz)^2 - (f_0/GHz)^2}{0.81} \tag{2.2}$$

There are a few problems that come along with using a hairpin probe that will need to be addressed before this can be put into practice. Hairpin probes create a floating sheath about them. In the off cycle of the pulse the sheath about the probe will collapse just as the sheath about the plasma does. This necessitates the implementation of a change in how data is extracted. Fortunately a method has already been created for doing this[35], which we will look toward when we take measurements. At the time of the writing of this thesis our hairpin probe was not yet operational; we do plan to use data taken with it in conjunction with the VI probe to model the sheath fluctuations through the pulse cycle.

CHAPTER

3

EXPERIMENT

Chapter 2 explained how the experimental apparatus is designed, detailing the chamber, electrodes, and generators. Concluding with the instrumentation used to probe the plasma. This chapter details how the results were processed. Examining the transient regions of the pulse cycle and noting changes in the sheath thickness as a result of plasma conditions.

3.1   Data analysis

Time dependent VI measurements were taken to analyze how the plasma responded to different set parameters. The default parameters were as follows: the 28.476 MHz pulsed generator was set to 200 W and pulsed at 500 Hz with a 50% duty cycle, the 12.88 MHz CW generator was set to 50 W, argon was used as the feed gas and pressure was maintained at 100 mTorr. The beginning of each section will detail the modifications made to these settings. The VI probe was set to measure the frequency of the12.88 MHz CW generator, since it was always on there would always be a signal to measure. At the probe's fastest sample rate it is capable of taking a measurement every 7.8 μs. This results in less than five data points during the transient region of the pulse cycle. Fortunately, the probe is capable

of taking measurements over several pulse cycles; using the code in Appendix B, the data was garnered to represent one pulse cycle with data sampled approximately every 0.2 μs, for a 500 Hz pulse frequency.

The VI probe calculates the impedance of the plasma which is used to calculate the sheath thickness.

The VI probe measures the entirety of the plasma; meaning, the impedance of the plasma is made up of the bulk plasma impedance plus the impedance of both sheaths given as Eq. 3.1.

$$Z_{plasma} = Z_{bulk} + 2Z_{sheath} \tag{3.1}$$

For an RF CCP the electric field is typically much smaller in the bulk than the sheaths of the plasma. The electric field of these regions is:

$$E_{sheath} = \frac{J_{Tx}}{j\omega\epsilon_0} \tag{3.2}$$

$$E_{bulk} = \frac{J_{Tx}}{j\omega\epsilon_p} \tag{3.3}$$

It is noted that the only difference in these equations is ϵ. Typically $\epsilon_p < 0$ and $|\epsilon_p| \gg \epsilon_0$ resulting in the impedance of the bulk being small compared to the impedance of the sheaths. ϵ_p is the plasma dielectric constant and is

$$\epsilon_p = \epsilon_0 \left(1 - \frac{\omega_{pe}^2}{\omega^2}\right) \tag{3.4}$$

Where ω_{pe} is the plasma dielectric constant and is dependent on the electron density[26] which we were unable to measure in the transient regions as detailed in 2.3.3. So it is assumed that the plasma is typical with the intention of proving this after hairpin probe measurements are taken.

In these calculations relative sheath thicknesses is acceptable. Thus we can simplify Eq. 3.1 by removing the bulk impedance term and dividing the impedance at the current point by the point where the 27 MHz generator turned on.

$$\frac{Z_{plasma}}{Z_{plasma0}} = \frac{Z_{sheath}}{Z_{sheath0}} \tag{3.5}$$

Impedance is the combination of the resistance and the reactance. Resistance and reactance

can be expressed in terms of sine and cosine as:

$$R = Z \cos \theta \tag{3.6}$$

$$X = Z \sin \theta \tag{3.7}$$

Reviewing data taken at several different settings it was found that the smallest angle measured was 77°. To determine how significant this was Eq. 3.6 was divided by Eq.3.7, while using 77° for θ. The result was 0.3057, which when compared to the lowest measured impedance of 84 Ω, was found to be a mere 0.3%. So resistance is taken to be a constant with respect to time, leaving just the reactance. Reactance is also known to be equal to Eq. 3.8.

$$X = \frac{s}{\omega \epsilon_0 A} \tag{3.8}$$

Where ϵ_0 is the permittivity of free space, A is area of the electrode, ω is the frequency being measured, and s is sheath thickness, our quantity of interest. ω is set to 12.88 MHz so that there will be data for the entire duration of the pulse, making it a constant. All of the variables other than the sheath thickness are constants and can thus be negated from the equation. Resulting in Eq.3.9.

$$\frac{Z_{plasma}}{Z_{plasma0}} = \frac{s}{s_0} \tag{3.9}$$

3.2   Transients

Upon plotting the reactance it was noticed that the data followed an exponential trend, so the natural log of the reactance was taken. Zooming in to look at the transition between the 28.476 MHz pulsed generator being off to on it was noted that there are four distinctive regions, as seen in Fig. 3.1. A, the background sheath when 28.476 MHz pulsed generator is off. B, the electron temperature decay; C, the electron density decay. And, D, the background sheath when 28.476 MHz pulsed generator is on. The transients are closely examined to determine the exact location each region begins and ends.

   The regions found in Fig. 3.1 are corroborated with experimental results from [28, 25] and theoretical results from [13]. As seen in figure 3.2 the electron temperature decays away much faster than the electron density. It is noted that Fig. 3.2 is of a chlorine plasma and Fig. 3.1 is an argon plasma. Fig.ArCl compares the electron temperature decay and electron density decay for an argon plasma to a chlorine plasma[41]. It is noted from this that the
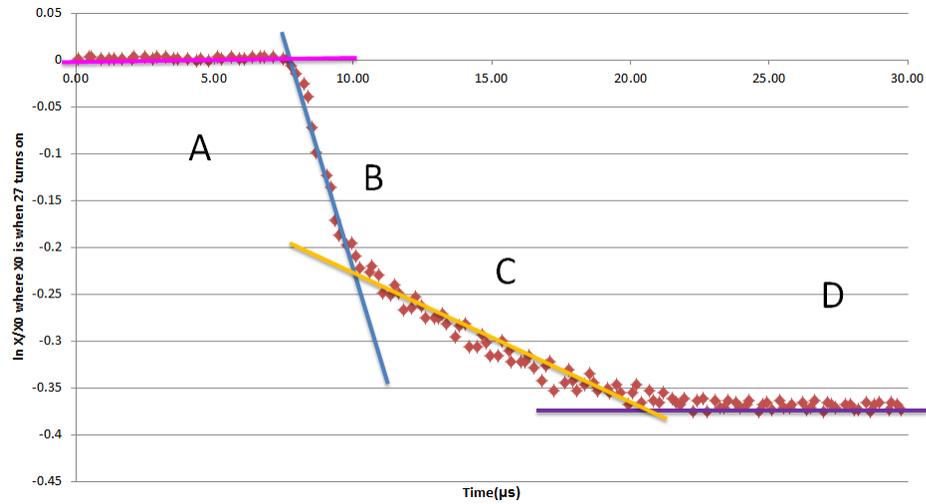
Figure 3.1: Transient region between off and on.

electron temperature decays much faster than the electron temperature for both argon and chlorine.
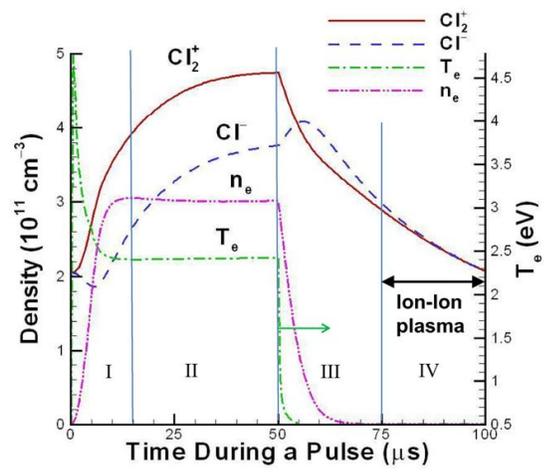
Figure 3.2: Pulsed plasma model of chlorine gas, detailing the evolution of electron temperature and density as a function of time[13].

The on to off transient region is not as distinctive. The on to off transient was zoomed
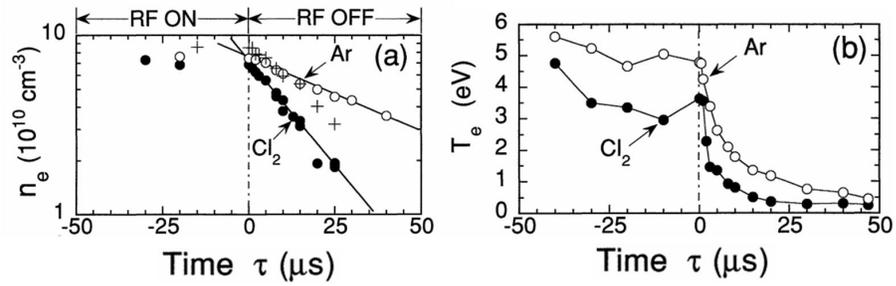
Figure 3.3: "Temporal variations in (a) electron density n_e, (b) electron temperature T_e" of pulsed chlorine and argon plasmas[41].

into and then the data was inverted so it could be directly compared to the off to on transient region, as seen in Fig. 3.4. While being comprised of regions with the same slopes as in the off to on transient, the on to off transient has some additional regions. These regions are believed to be caused by voltage fluctuations causing an over shoot as discussed in Chapter 1. This paper will only be investigating the off to on transient region with the intention of characterizing the effect of pulse frequency, power, pressure, and gas composition on sheath thickness.
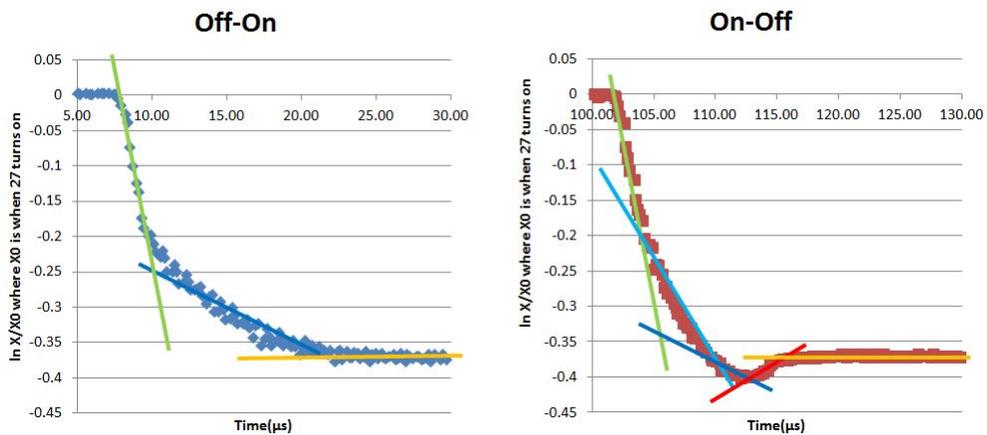
Figure 3.4: Left: Same graph as in Fig. 3.1. Right: On-Off transient region. All lines that match in color between the two graphs also match in slope.

3.2.1 Power Variations

Pulsed Generator Power Variations

The power of the 28.476 MHz pulsed generator was varied from 25 W to 100 W in 25 W steps then to 400 W in 100 W steps while pressure was kept at 50 mTorr. Fig. 3.5 and Fig. 3.6 show the value of the slope with changing pressure in regions B and C, respectively. Fig. 3.7 shows the average difference in the sheath thickness between when the 28.476 MHz pulsed generator turned on to region D, for the same plasma. A graph of the slopes in region D is excluded since region D is made up of approximately flat lines with an average slope value of approximately 5×10^{-5}.

Examining Fig. 3.5, it is noted that electron temperature is more affected by changes in power from the 28.476 MHz pulsed generator when the power is below 200 W. Fig. 3.6 demonstrates that the electron density is far more affected by changes in power of the 28.476 MHz pulsed generator when the power is above 200 W.

Looking at Fig. 3.7, the average value of the background sheath, region D nearly perfectly mirrors region B. It is concluded that the electron temperature dominates the overall change in sheath thickness with respect to changes in the power of the 28.476 MHz pulsed generator. While examining Fig. 3.5, and Fig. 3.6, it might look obvious that electron temperature should dominate over the change in sheath thickness because its slope values are larger by a factor of ten, it is noted that both electron temperature and electron density are changing in both regions as seen in Fig. 3.2. Therefore the trend in the slope per each region must be examined to determine which dominates the changes in sheath thickness .

It should be noted that Fig. 3.6 does not have a value for 25 W. This is because region C could not be found at 25 W. As power increases, the distance between regions A and D increase. For 25 W the difference between regions A and D is 0.01, whereas for 400 W it is 0.12. Subsequently the time to travel from region A to D is significantly shorter for lower power. For 25 W, this space is covered in 0.64μs, corresponding to five data points, which fit perfectly on one line. It was assumed that this line represented region B due to its large value as compared to the value of the 50 W slope in region C. Furthermore, the width of both background sheaths, region A and region D, are constant with pressure and power, giving a value of 0.01. It is thus believed that region C for 25 W is completely sacrificed for region B similarly to what was seen for changing pulse frequency in 3.2.3
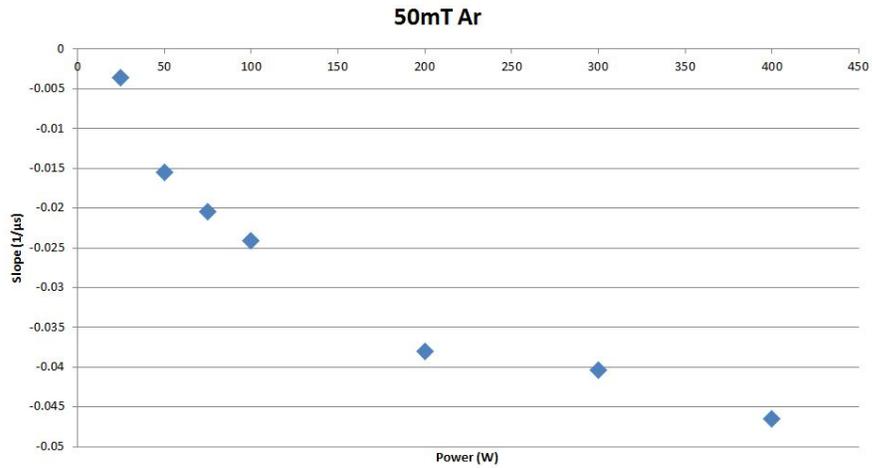
Figure 3.5: Region B for a 50mT argon plasma in a power sweep of the 28.476 MHz pulsed generator.
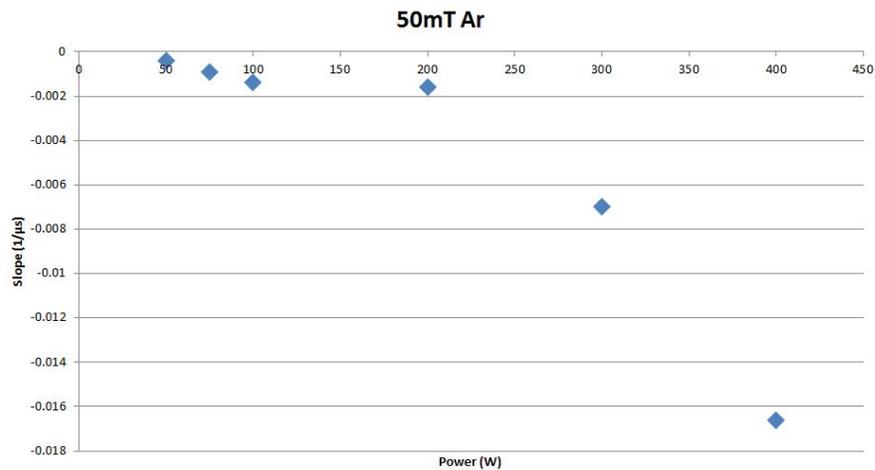
Figure 3.6: Region C for a 50mT argon plasma in a power sweep of the 28.476 MHz pulsed generator.

CW Generator Power Variations

The power of the 12.88 MHz CW generator was varied from 25 W to 200 W in 25 W steps. Just as in the previous generator power sweep, region C has no effect on the background sheath thickness. Fig. 3.8 shows region B and region D. The opposite trend is seen with increasing
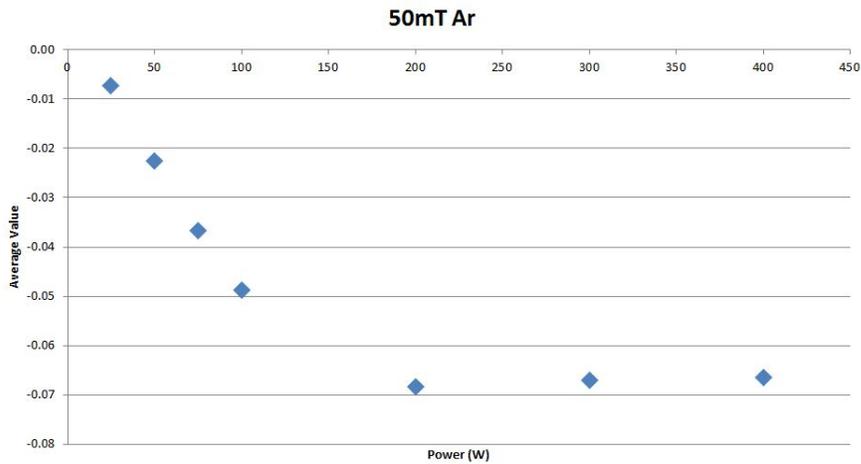
Figure 3.7:   Region D for a 50mT argon plasma in a power sweep of the 28.476 MHz pulsed generator.

the power of the 12.88 MHz CW generator as was seen in Fig. 3.7 for varying the power of the 28.476 MHz pulsed generator. Depending on generator frequency, different parts of the plasma are affected by changes in the power of that generator. High frequency generators like the 28.476 MHz pulsed generator deposit most of their power into the sheaths of the plasma. Thus increasing the power of the generator increases the width of the sheath. Lower frequency generators like the 12.88 MHz CW generator deposit most of their power into the bulk of the plasma. When the bulk of the plasma increases, the sheath must decrease to make room for it. Therefore a decrease in sheath thickness is seen with increasing the power of the 12.88 MHz CW generator.

It is noted that at 25 W the slope is significantly sharper than at any other point and that this value does not fit the trend line that the rest of the slopes create. This is believed to be a time balancing issue as it is noted that 25 W does fit the trend line of the average sheath thickness value. Additionally it is noted that, 25 W spends 0.92 μs in region 1 where all of the rest spend over 2.5 μs. And , while their electron temperature does still change in region C it is noted from Fig. 3.2 that the change in electron temperature does quickly go to zero allowing for the assumption that the time spent in that region is the entire change in electron temperature.
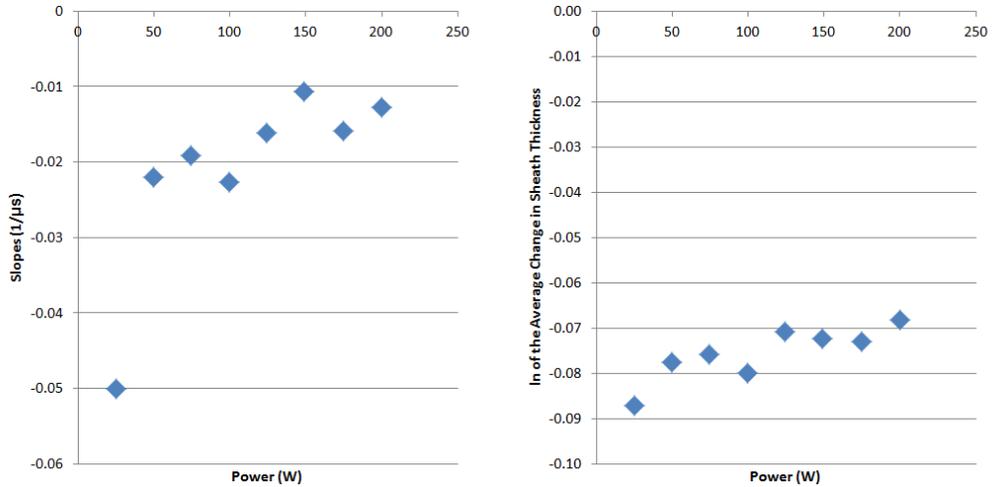
Figure 3.8: Left: Region B for an argon plasma in a power sweep of the 12.88 MHz CW generator. Right: Region D for an argon plasma in a power sweep of the 12.88 MHz CW generator.

3.2.2 Pressure Variations

The purpose of this section is to look at pressure variations but to also detail how the adjustment of multiple parameters affects the plasma. Pressure was varied between 50, 100, and 200 mTorr, using argon and oxygen as flow gases. While also varying the power of the 28.476 MHz pulsed generator from 25 W to 100 W in 25 W steps then to 400 W in 100 W steps.

Investigating pressure's effect on slopes for an argon plasma, a few interesting things come to light. Fig. 3.9 shows region B at 50, 100, and 200 mTorr. First, there is a significant change in the value of the slopes that occurs between 100 and 200 W. Looking back at Fig. 3.7 it can be seen that starting at 200 W the background sheath become constant. It is believed that the minimum sheath thickness possible for argon is achieved at 200 W; therefore, adding more power does nothing for the system.

The other notable trend is that the slopes for 100 mTorr are not less than the slopes for 50 mTorr. This is because 100 mTorr spends more time in region B than either 50 or 200 mTorr as seen in Table 3.1. It is unclear why 100 mTorr is an anomaly but it is clear after examining Fig. 3.10 that these two inconsistencies worked together so that 100 mTorr still follows the same general sheath thickness trend.

Switching to look at oxygen, in Fig. 3.11 it can be seen that a maximum electron density
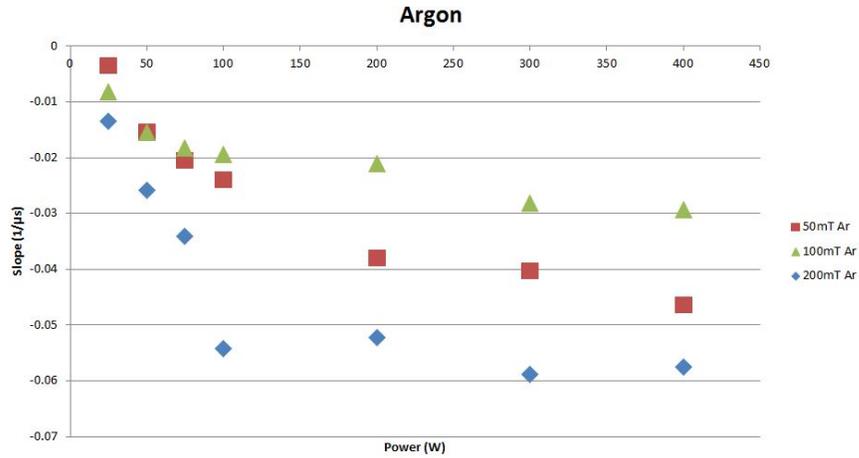
Figure 3.9: Region B for an argon plasma in a power sweep of the 28.476 MHz pulsed generator.

Table 3.1: Time(μs) spent in region B.

	$50mT$	$100mT$	$200mT$
$25W$	0.64	2.20	1.56
$50W$	1.10	1.88	1.88
$75W$	1.10	2.34	1.74
$100W$	1.10	2.66	1.56
$200W$	1.42	3.44	1.88
$300W$	1.56	2.52	1.74
$400W$	1.56	2.52	1.74

is never reached. Also, the slopes in region B are unaffected by pressure, consequently neither is the average change in background sheath thickness in region D.

Pressure and gas were not varied for the 12.88 MHz CW generator because varying them for the 28.476 MHz pulsed generator power sweep did not turn up any surprising data; thus it was inferred that changing these conditions would have a similar reaction with another power sweep.

36
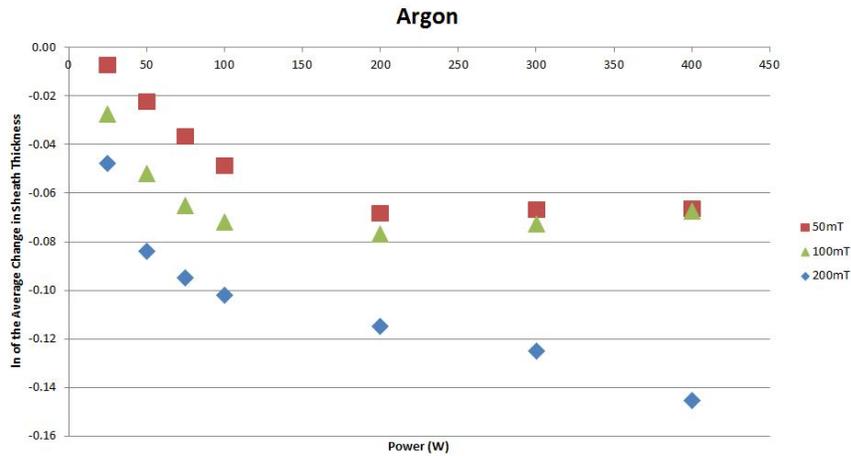
Figure 3.10: Region D for an argon plasma in a power sweep of the 28.476 MHz pulsed generator.
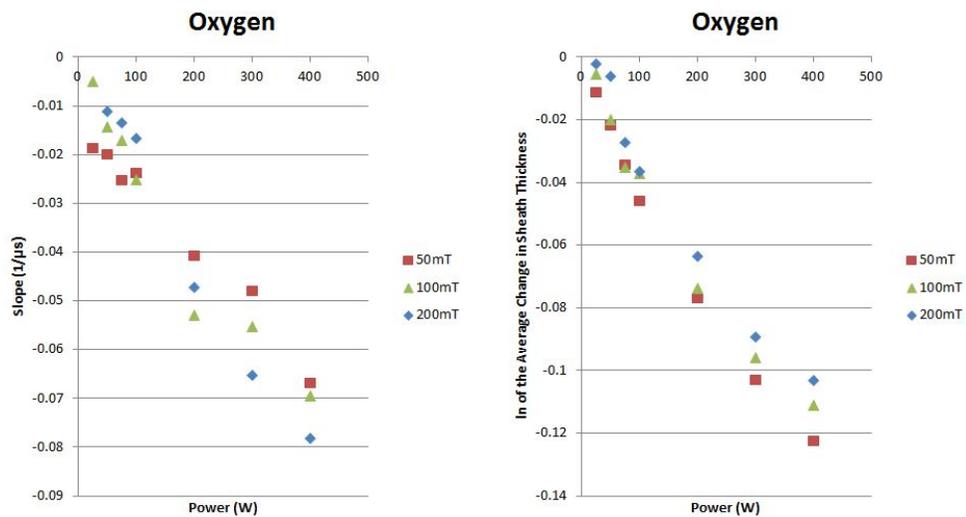
Figure 3.11: Left: Region B for an oxygen plasma in a power sweep of the 28.476 MHz pulsed generator. Right: Region D for an oxygen plasma in a power sweep of the 28.476 MHz pulsed generator.

3.2.3 Pulse Frequency Variations

In examining the changes in slope for several experiments it was noted that except for a couple of outliers, the time that electron temperature dominates is a couple of micro seconds. Remembering that in 3.2.1 region C completely disappeared when the pulsing generator is at low power, it was proposed that the time electron temperature dominated was fixed. To test this, the pulse frequency was varied from 500 Hz to 10 kHz.

For this experiment the pulse frequency was varied from 500 Hz to 10 kHz. In region
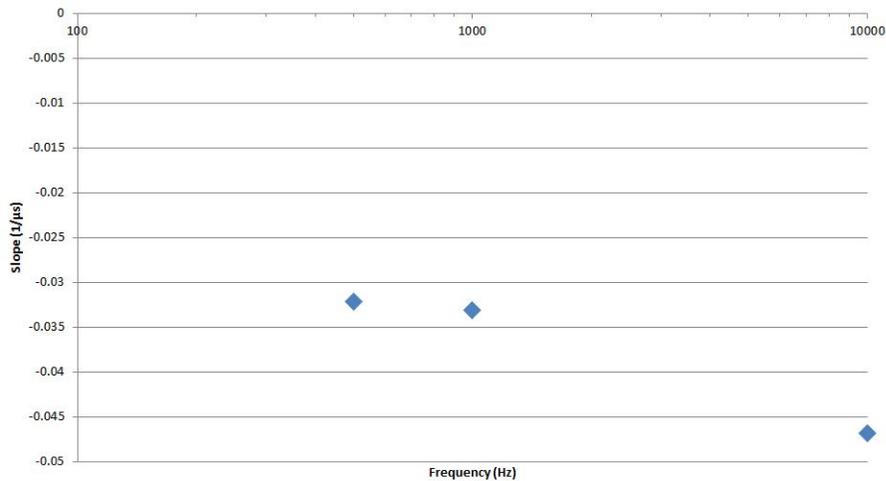
Figure 3.12:   Change in slope in region B with respect to changing pulse frequency.

B, the slope increased as pulse frequency increased, as shown in Fig. 3.12. The time spent in the region B was approximately constant across the range of pulse frequencies. With electron temperature quickly decaying after it is no longer dominant, this means that slopes are a useful means of comparison and that the a conversion to average change in sheath thickness is not needed.

Looking at region C, Fig. 3.13 left, it appears that higher frequencies have far more of an affected on electron density than lower frequencies. This graph does not paint the whole picture. Electron density changes throughout the entire pulse cycle; Fig 3.2, shows that the change in electron density appears to have a linear. Meaning if the slope for region C is multiplied by the entire transient time, an approximate picture for how electron density affects the sheath thickness. This calculation is performed and shown in Fig. 3.13 right. Examining this figure shows there is no evident trend. Although, it is noted that the points do look similar to what Overzet and Verdeyen saw in Fig. 1.7. It is further noted that Overzet and Verdeyen used a helium silane mixture and this experiment used argon [30].

Region D, Fig. 3.14, shows a drop in the average sheath thickness, similar to that seen in region B. It can be concluded that increasing the pulse frequency increases the change in electron temperature; as a result, increasing the average sheath thickness.
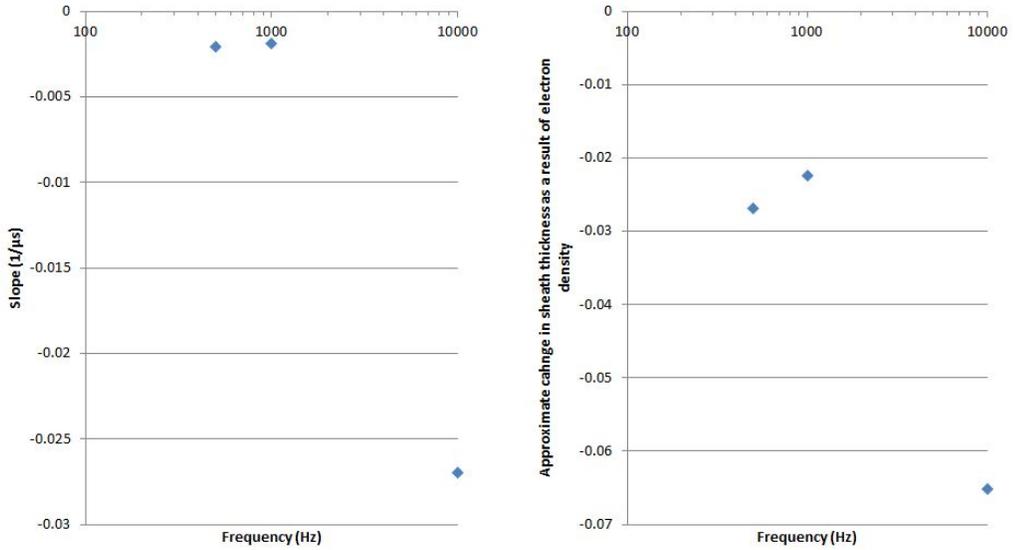
Figure 3.13:   Left: Change in slope in region C with respect to changing pulse frequency. Right: Approximate in sheath thickness as a result of electron density with respect to changing frequency.
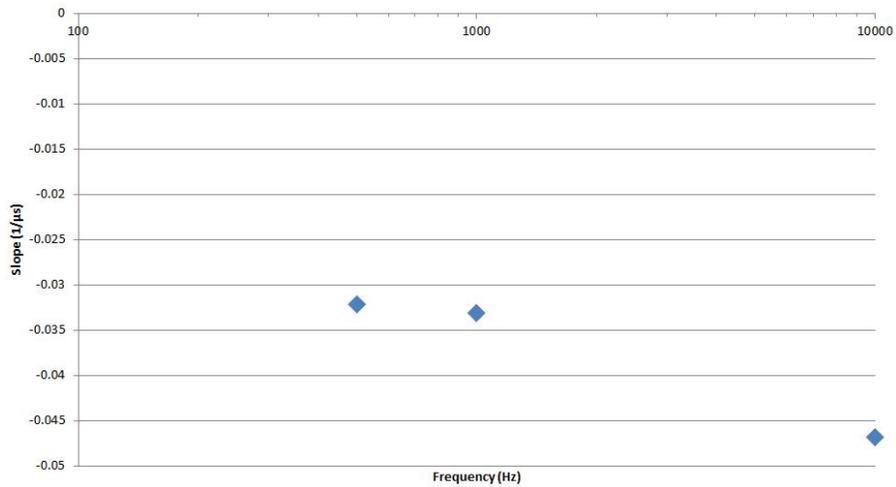
Figure 3.14:   Change in average sheath thickness slope in region D with respect to changing pulse frequency.

3.2.4   Gas Mixing

Several experiments have been performed for the mixing of gasses in a pulsed plasma. The work done by Neyts et. al. on mixed gas CCPs was particularly interesting. She added

hydrogen to an argon plasma and saw an increase in electron density for small quantities of hydrogen and then a significant drop for increased hydrogen[11], Fig. 1.4. It was postulated that the same thing could be seen for an argon oxygen plasma because both gases have vibrational states.

Data was initially taken with a pure argon plasma. Then oxygen was added starting at 3.125% and the oxygen partial pressure was doubled until the plasma was half oxygen. This experiment was run at 50, 100, and 200 mTorr to verify the trend and look for a pressure dependence. Examining region D, it is obvious there is no variation in trend with changing pressure other than for a purely argon plasma. Fig. 3.15 shows a sudden drop in average change in sheath thickness from 0 to 3.125% oxygen then a slight bump at 6.25% oxygen followed by a steady decrease in average sheath thickness with increasing oxygen concentration.
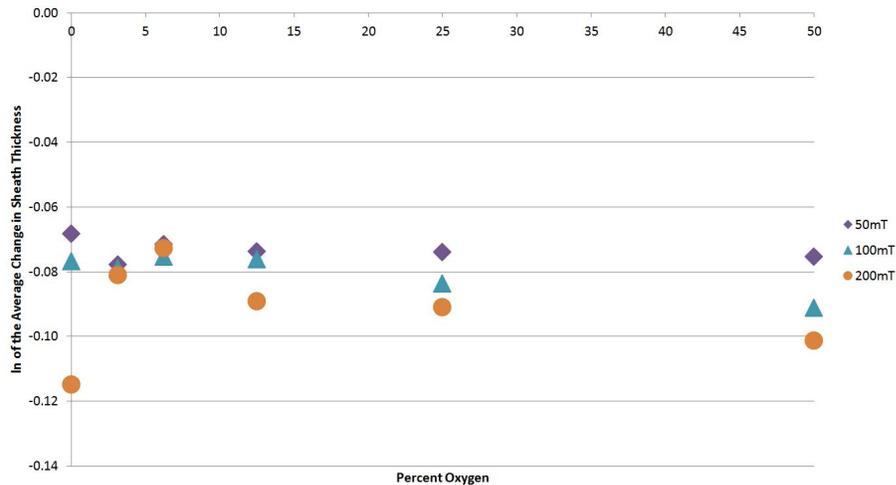
Figure 3.15: Region D, bump in average sheath thickness seen with increasing oxygen partial pressure.

It could be suspected that these results are due to a random error in measurement. First off, to cut down on error, all data that is directly compared was taken at the same point in time. Thus issues such as outgassing of the chamber are irrelevant. To determine the fluctuation in results between samples, six samples were taken of an argon plasma at 100 mT with the 28.476 MHz pulsed generator at 200 W and 500 Hz with a 50% duty cycle, and the 12.88 MHz CW generator at 50 W. The average value of the average change in sheath

thickness from the begining of the pulse to region D was -0.0876 with a standard deviation of 0.00319 resulting in an uncertainty of 3.65%. A couple of the data points fall within this uncertainty. However, this trend was seen at multiple pressures and on multiple days, so the only possible conclusion is that this trend is true or there exists a systematic error.

It is concluded that what is seen in Fig. 3.15 is not an error. Region C, Fig. 3.16, the region dependent on electron density showed the same trend as Neyt et. al. [11], while region B showed no correlation.
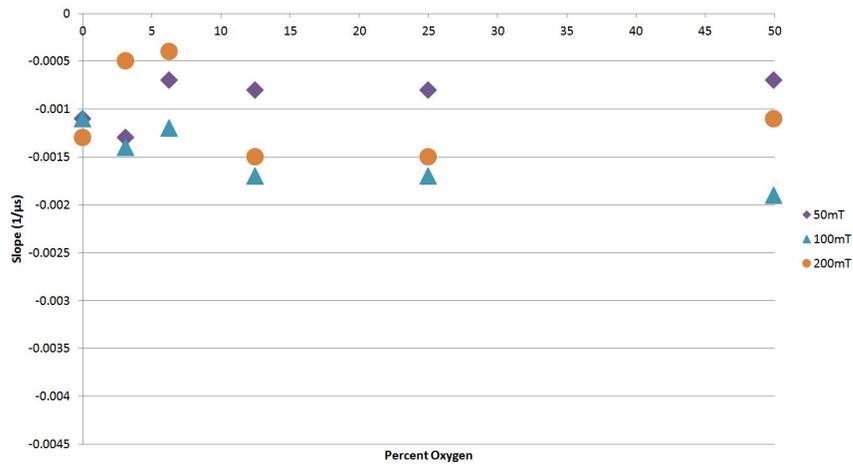
Figure 3.16:   Bump in electron density seen with increasing oxygen partial pressure.

CHAPTER

4

CONCLUSIONS AND FUTURE WORK

In the previous chapter the experiments which were performed were discussed. Frequency and gas concentration were adjusted to look for similar results as seen in previously published papers for different pulsing systems. Power and pressure was adjusted so the trends could be noted to be used as a check for future computational work. This chapter will make conclusions about the results seen in chapter three, going on to purpose future work for the project.

In all power varying experiments, the average change in sheath thickness was predominately the result of a change in electron temperature. The change in temperature was dependent on the frequency of the generator. High frequency generators deposit most of their power into the sheaths of the plasma while lower frequency generators deposit most of their power into the bulk of the plasma. As a result, increasing the power of the 28.476 MHz pulsed generator, resulted in an increase in temperature. While increasing the power of the 12.88 MHz CW generator, resulted in an decrease in temperature.

Continuing the investigation of power effects on the plasma, the effect of changing power and pressure was examined for both an argon and oxygen plasma. For argon, changing pressure seems to have a significant effect on the change in average sheath thickness,

while oxygen is unperturbed. It is believed that oxygen has a collisionless sheath in these experiments and that argon has already made the transition from a collisionless to a collisional sheath. To investigate this, the equations for sheath thickness were derived for a Child Law collisionless sheath and a collisional sheath:

$$s_m^{1/2} = 0.82 * \epsilon_0 * \sqrt{\frac{2e}{M}} * \frac{V^{3/2}}{J_i} \tag{4.1}$$

$$s_m^{5/2} = 0.82 * \epsilon_0 * \sqrt{\frac{2e}{M}} * \frac{V^{3/2} \lambda_i^{1/2}}{J_i} \tag{4.2}$$

The voltage was acquired from VI probe measurements and J_i, the ion current, was acquired from Langmuir probe measurements. While taking Langmuir probe measurements in the transients of the plasma had proven fruitless, taking measurements of the settled plasma were more promising. Time resolved Langmuir probe measurements were taken after the transient regions when the 28.476 MHz pulsed generator was on or off. This was done so the natural log of the average change in sheath thickness could be calculated and compared to the VI probe results and identify whether the VI probe data indicated a collisionless or collisional sheath.

Unfortunately this endeavor proved to be in vain. Results for an argon plasma were not of the same order of magnitude as those gathered with the VI probe, and the measurements for oxygen had a negative ion current. Based on the data gathered from the Langmuir probe for this experiment, and taken by colleagues for their experiments, it appears that something is wrong with the Langmuir probe installed in the chamber. It is necessary to repeat these experiments with a time resolved hairpin probe, or after identify and fixing what is wrong with the Langmuir probe, to confirm that changes in collisionality of the sheath is what causes the differences in the plasmaâĂŹs response to pressure.

It is noted that the argon plasmaâĂŹs change in sheath thickness becomes constant for a 50 and 100 mTorr plasma after 200 W. It is believed that at this point the sheath has reached its minimum possible thickness and cannot shrink any further. Further tests using OES are needed to verify this. OES data would be possible to take at this point because the pictures would occur after the transient region, so the decay time of argon would not be a problem.

Pulse frequency was varied and a positive correlation was seen in electron temperature. As the pulse frequency increases, if duty cycle remains constant, the time for electrons to diffuse is decreased. Resulting in more electrons being present at the beginning of the

pulse cycle at higher frequencies, as discussed in 1.4. Ultimately, this causes higher electron temperatures at higher pulse frequencies.

A correlation was also seen between the electron density of an argon plasma and a helium silane plasma with respect to frequency[30]. Both showed a local extrema in electron density at a pulse frequency around 1000 Hz. This was highly unexpected since the gasses have little in common. It is proposed that this experiment be repeated with another, non-noble gas to further determine what causes the dip in electron density at around 1000 Hz.

In examining the gas mixing data, it was decided to divide the data into two groups: above and below 10% oxygen partial pressure. Below 10%, the data corresponds quite well with Neyts et. al. work[11]; there was a bump in electron density with a small addition of diatomic gas and upon increasing pressure this bump disappeared.

Neyts et. al. concluded that the bump in electron density was because at low hydrogen partial pressures there is a low fraction of high energy electrons, caused by the introduction of the vibrational state of hydrogen. Interactions between an electron and a hydrogen molecule induce a vibrational state via an inelastic collision, depleting energy from the electron, and preventing their rise to high energy. Low energy electrons do not have enough energy to escape the plasma bulk to be lost to the walls causing the electron density to increase. While at higher hydrogen partial pressures there are more high energy electrons thus more electrons are lost to the walls[11].

Oxygen also has a vibrational state[5] like hydrogen. At 3.125% partial pressure oxygen with a pressure of 50 or 100 mTorr, it is believed that these vibrational states have split the electrons into a high and low energy region, like with Netys' âĂŹ work, causing the electrons to become trapped in the plasma, increasing the electron density. At 6.25% the energy of the electrons has increased and the high energy electrons are no longer trapped in the plasma causing the average electron temperature to drop. At 200mT the electrons are no longer split into two groups at low partial pressure and are simply lost to the walls, as Neyts et. al. saw[11].

Above 10% the sheath thickness increases regardless of pressure. This is leads to an interesting effect at 50 and 100 mTorr. ArgonâĂŹs change in sheath thickness is greater than oxygen, as seen in 3.2.2. Despite this, somehow, at 50 and 100 mTorr, a larger change in sheath thickness is seen for an argon-oxygen plasma than either is able to create alone. It is unknown why this is happening and it needs to be further investigated.

It is the goal of this project to correlate measured plasma conditions to empirical models

as a means of developing feed-forward/feed-backward control to be later combined with intelligent power delivery algorithms to make smart pulsing generators. In this paper the variance of the sheath has been characterized for varying plasma conditions. An empirical model has already been developed to characterize the plasma. Similar models have already been tested with a pulsed plasma and shows good corroborate with experimental results[39]. Moving forward with the project it is necessary to take time resolved hairpin probe measurements to corroborate the model with a pulsed plasma.

REFERENCES

[1] Chemical elements listed by ionization energy. http://www.lenntech.com/periodic-chart-elements/ionization-energy.htm.

[2] Frequency scanning v/i probe ®. Technical report, MKS.

[3] Pulsed rf sources. http://www.microwaves101.com/encyclopedias/pulsed-rf-sources.

[4] J.-L. Dorier A. A. Howling and Ch. Hollenstein. Negative ion mass spectra and particulate formation in radio frequency silane plasma deposition experiments. *Applied Physics Letters*, 62(12):1341, 1993.

[5] Michael Allan. Measurement of absolute differential cross sections for vibrational excitation of 0 2 by electron impact. *Journal of Physics B: Atomic, Molecular and Optical Physics*, 28(23):5163, 1995.

[6] Laurent Sansonnens Antoine Descoeudres and Ch Hollenstein. Attachment-induced ionization instability in electronegative capacitive rf discharges. *Plasma Sources Science and Technology*, 12(2):152, 2003.

[7] R. W. Boswell and D. Henry. Pulsed high rate plasma etching with variable si/sio2 selectivity and variable si etch profiles. *Applied Physics Letters*, 47(10):1095, 1985.

[8] Ch Hollenstein L Sansonnens C Courteille, J-L Dorier and A A Howling. Partial-depth modulation study of anions and neutrals in low-pressure silane plasmas. *Plasma Sources Science and Technology*, 5:210, 1996.

[9] M.J. CARVALHO and G. KLEIN. Luminescence decay in condensed argon under high energy excitation. *Journal of Luminescence*, 18(1):487–490, 1979.

[10] William Crookes. *Radiant matter : a resume of the principal lectures and papers of Prof. William Crookes, on the 'fourth state of matter'*. James W. Queen & Co., 1881.

[11] A. Bogaerts R. Gijbels E. Neyts, M. Yan. Pic-mc simulation of an rf capacitively coupled ar/h2 discharge. *Nuclear Instruments and Methods in Physics Research Section B: Beam Interactions with Materials and Atoms*, 202:300–304, April 2003.

[12] P. Awakowicz E. Semmler and A von Keudell. Heating of a dual frequency capacitively coupled plasma via the plasma series resonance. *Plasma Sources Science and Technology*, 16(4):839, 2007.

[13] Demetre J. Economou. Pulsed plasma etching for semiconductor manufacturing. *Journal of Physics D: Applied Physics*, 47(30):303001, 2014.

[14] Valery Godyak. Low pressure rf plasma sources for industrial applications (icp versus ccp). August 2011.

[15] Dushyant Gupta. Plasma immersion ion implantation (piii) process-physics and technology. *International Journal of Advancements in Technology*, 2(4):471–490, 2011.

[16] Y. Hikosaka H. Sugai, K. Nakamura and M. Nakamura. Diagnostics and control of radicals in an inductively coupled etching reactor. *Journal of Vacuum Science and Technology A*, 13(3):887, 1995.

[17] J. D. Huba. Nrl plasma formulary, 2014.

[18] Impedance. *ALP System™Langmuir Probe Installation & User Guide*, 2.8 edition, 8 2011.

[19] G. Qiu J. L. Walsh J. J. Shi, J. Zhang and M. G. Kong. Modes in a pulse-modulated radio-frequency dielectric-barrier glow discharge. *Applied Physics Letters*, 93:041502, 2008.

[20] E. Y. Choueiri J. K. Ziemer and Daniel Birx. Trends in performance improvements of a coaxial gas-fed pulsed plasma thruster. In *Proc. of 25th International Electric Propulsion Conference, IEPC-97-040*, 1997.

[21] E.A. Cubbin J.K. Ziemer and E.Y. Choueiri. Performance characterization of a high efficiency gas-fed pulsed plasma thruster. In *33RD JOINT PROPULSION CONFERENCE AND EXHIBIT*, 1997.

[22] Takashi Yagisawa Kazunobu Maeshige, Gentaro Washio and Toshiaki Makabe. Functional design of a pulsed two-frequency capacitively coupled plasma in cf4/ar for sio2 etching. *Journal of Applied Physics*, 91(12):9494, 2002.

[23] Masaru Hori Kunimasa Takahashi and Toshio Goto. Control of fluorocarbon radicals by on-off modulated electron cyclotron resonance plasma. *Japanese Journal of Applied Physics*, 32:L1088, 1993.

[24] Irving Langmuir. Oscillations in ionized gases. *Proceedings of the National Academy of Sciences of the United States of America*, 14(8):627, August 1928.

[25] Mikhail V. Malyshev. *Advanced Plasma Diagnostics for Plasma Proccessing*. PhD thesis, Princeton University, 1999.

[26] Allan J. Lichtenberg Michael A. Lieberman. *Principles of plasma discharges and materials processing*. John Wiley & Sons, Inc., Hoboken, NJ:, second edition, 2005.

[27] Iain D. Boyd Michael Keidar and Isak I. Beilis. Electrical discharge in the teflon cavity of a coaxial pulsed plasma thruster. *IEEE Transactions on Plasma Science*, 28(2):376–385, 2000.

[28] Tetsu Mieno and Seiji Samukawa. Time variation of plasma properties in a pulse-time-modulated electron cyclotron resonance discharge of chlorine gas. *Japanese Journal of Applied Physics*, 34:L1079, 1995.

[29] L. J. Overzet. Why and how to pulse a plasma. http://www.utdallas.edu/ overzet/puls_-97/index.htm, October 1997.

[30] L. J. Overzet and J. T. Verdeyen. Enhancement of the plasma density and deposition rate in rf discharges. *Applied Physics Letters*, 48(11):695–697, 1986.

[31] J-L Raimbault J-M Rax M. M. Turner P. Chabert, P. Levif and M. A. LiebermanLieberman. Electron heating in multiple-frequency capacitive discharges. *Plasma Physics and Controlled Fusion*, 48(12B):B231, 2006.

[32] J.L. Subtil N. Damany P. Moutard, P. Laporte and H. Damany. Pressure effects on kinetics and decay processes in argon under selective photoexcitation. *The Journal of Chemical Physics*, 87:4576–4588, 1987.

[33] J Al-Kuzee R B Piejak and N St J Braithwaite. Hairpin resonator probe measurements in rf plasmas. *Plasma Sources Science and Technology*, 14:734–743, 2005.

[34] M.M. Abdel Rahman. Ion sources for use in research and low energy accelerators. *International Journal of Instrumentation Science*, 1(5):63–77, 2012.

[35] A. R. Ellingboe-I. Swindells S. K. Karkari, C. Gaman and J. W. Bradley. A floating hairpin resonance probe technique for measuring time-resolved electron density in pulse discharge. *Measurement Science and Technology*, 18(8):2649, 2007.

[36] Seiji Samukawa and Shuichi Furuoya. Time-modulated electron cyclotron resonance plasma discharge for controlling generation of reactive species. *Applied Physics Letters*, 63(15):2044, 1993.

[37] Seiji Samukawa and Kazuo Terada. Pulse-time modulated electron cyclotron resonance plasma etching for highly selective, highly anisotropic, and less-charging polycrystalline silicon patterning. *Jounal of Vacuum Science and Technology B*, 12(6):3300, 1994.

[38] Seiji Samukawa and Tsutomu Tsukada. Effects of electron temperature in high-density cl2 plasma for precise etching processes. *Applied Physics Letters*, 69(8):1056, 1996.

[39] Daniel Hoffman Steven Shannon and Matthew Miller. Determination of effective ion mass using multi-frequency in-line rf metrology. In *Bullitne of the American Physical Society*, volume 51, page 37, 2006.

[40] M. Surendra and D. B. Graves. Capacitively coupled glow discharges at frequencies above 13.56 mhz. *Applied Physics Letters*, 59(17):2091, 1991.

[41] K Nakamura T H Ahn and H Sugai. A new technology for negative ion detection and the rapid electron cooling in a pulsed high-density etching plasma. *Japanese Journal of Applied Physics*, 34(10B):L1405–L1408, October 1995.

[42] K Nakamura T H Ahn and H Sugai. Negative ion measurements and etching in a pulsed-power inductively coupled plasma in chlorine. *Plasma Sources Science and Technology*, 5(2):139, 1996.

[43] M. Hofmann R. Krĺucken-L. Oberauer W. Potzel J. Wieser T. Heindl, T. Dandl and A. Ulrich. The scintillation of liquid argon. *European Physics Letters*, 91:62002, 2010.

[44] Z. Lj. Petrovicť T. Kitajima, Y. Takeo and T. Makabe. Functional separation of biasing and sustaining voltages in two-frequency capacitively coupled plasma. *Applied Physics Letters*, 77(4):2000, 2000.

[45] T. Kitajima T. Ohmori, T. K. Goto and T. Makabe. Negative charge injection to a positively charged sio2 hole exposed to plasma etching in a pulsed two-frequency capacitively coupled plasma in cf4 /ar. *Applied Physics Letters*, 83(22):4637, 2003.

[46] Joseph John Thomson. Xl. cathode rays. *The London, Edinburgh, and Dublin Philosophical Magazine and Journal of Science*, 44:293, 1897.

[47] Masaaki Okubo Tomoyuki Kuroki, Shingo Tanaka and Toshiaki Yamamoto. Low pressure pulse-modulated and radio-frequency plasma for cf 4 decomposition. In *In Industry Applications Conference, 2005. Fourtieth IAS Annual Meeting. Conference Record of the 2005*, volume 4, pages 2900–2905, 2005.

[48] S. V. BOBASHEV V. A. ANKUDINOV and E. P. ANDREEV. Measurement of lifetimes of excited states of the hydrogen atom. *Journal of Experimental and Theoretical Physics*, 48:40–49, 1965.

[49] Y. Kubo L. Ogawa Y. Watanabe, M. Shiratani and S. Ogi. Effects of low-frequency modulation on rf discharge chemical vapor deposition. *Applied Physics Letters*, 53(14):1263, 1988.

APPENDICES

APPENDIX

A

OPTICAL EMISSION SPECTROSCOPY CODE

A.1 Picture Creation Code

The pictures taken by Pi-Max were saved as code thus to look at the picture of the plasma again a code was written that would reconstruct the picture as well as place a cartoon figure at the bottom detailing when in the pulse cycle the photo was taken. These photos could then be strung together to form a movie or examined individually as seen in figure A.1.

The following code was used for two things. First the code was used to find the minimum and maximum intensity among all photos, the commented out lines. Then to convert the code back into pictures using a constant color intensity scale.

```
clear all
close all
clc
```
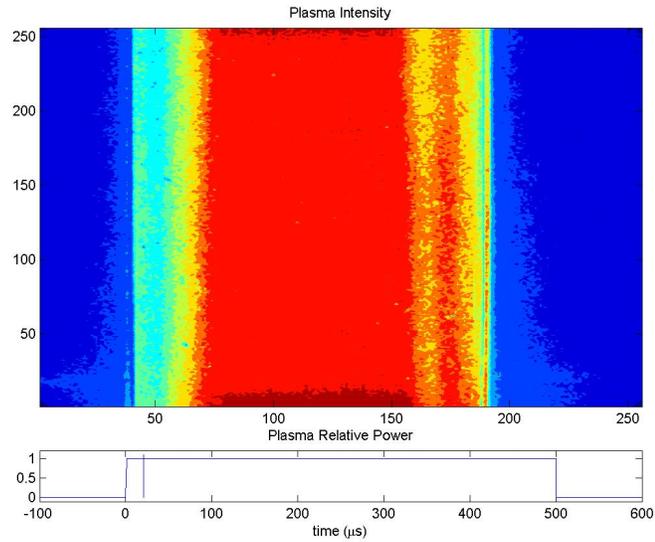
Figure A.1:   Photo of an argon plasma 20μs after the begining of the pulse.

```
z=4; % How coarse your output contour is (2^n)
p = 1024;
t = p^2; % Total pixils

A = zeros(1024,1024);
B = zeros(t,3);

firstfile = 0; % Number of first file
lastfile = 100; % Number of last file

xplot1 = [1:13];
xplot2 = [40:10:480];
xplot3 = [481:500];
xplot4 = [501:555];
xfill1 = [-100:0];
xfill2 = [14:30];
xrefdata = [xplot1];
```

```
xplotdata = [xfill1,xrefdata,xfill2];
yplot1 = ones(1,length(xplot1));
yplot2 = zeros(1,length(xplot4));
yfill1 = zeros(1,length(xfill1));
yfill2 = zeros(1,length(xfill2));
yrefdata = [yplot1];
yplotdata = [yfill1,yrefdata,yfill2];


% minimum = 1000;
% maximum = 0;


for n=firstfile:lastfile
     file = sprintf('100mT%d.csv',n);
     B = importdata(file,',');
     for m=1:t
         j=m;
         r = B(j,2);
         c = B(j,1);
         v = B(j,4);
         A(r,c) = v;
         % if (v < minimum)
             % minimum = v;
             % end
             % if (v > maximum)
             % maximum = v;
          % end
     end
     C = zeros(p/z,p/z);
     for u=1:p/z
         for v=1:p/z
             C(u,v) = A((p+1)-u*z,v*z);
         end
     end
```

53

```
        clf

        fig = figure(1);
        subplot(100,1,1:80)
        contourf(C,'LineStyle','none');
        caxis([ 389 53165 ])
              % Change these numbers based on minimum and maximum...
              intensites
        title('Plasma Intensity')
        subplot(100,1,90:100)
        plot(xplotdata,yplotdata)
        axis([-100 600 -.1 1.2])
        line([xrefdata(n+1) xrefdata(n+1)],[0 1.1])
        title('Plasma Relative Power')
        xlabel('time (\mus)')
        jpeg = sprintf('%d.jpeg',n);
        saveas(fig,jpeg);
end

% minimum
% maximum
```

A.2   1D Intensity Code

The code used to compile the 1D intensity line was built upon the same code used to create the photos. These were written as two separate codes because the code used to create the photos had a significant cost created by constructing the cartoon. The code calculates the second derivative and log of the intensity then plots it and exports the data to a spreadsheet.

```
clear all
close all
clc
```

```matlab
p = 1024;
t = p^2;    % Total pixils

A = zeros(1024,1024);
B = zeros(t,3);

firstfile = 0;       % Number of first file
lastfile  = 100;     % Number of last file
%lastfile = 33;

filename = 'logData.xlsx';
filename2 = 'd2IData.xlsx';

for n=firstfile:lastfile
    file = sprintf('100mT%d.csv',n);
    B = importdata(file,',');
    for m=1:t
        r = B(m,2);
        c = B(m,1);
        v = B(m,4);
        A(r,c) = v;
    end

    figInset = A(1:800,1:800);
    colMean = mean(figInset);

    L = log(colMean);
    d2I = zeros(1,length(L)-2);
    for loc=1:length(d2I)
        d2I(loc) = colMean(loc)+colMean(loc+2)-colMean(loc+1);
    end

    clf
```

```
        fig = figure(1);
        plot(L)
        title('natural log of intensity')
        jpeg = sprintf('log%d.jpeg',n);
        saveas(fig,jpeg);
        xlRange = sprintf('A%d',n+1);
        xlabel('Position');
        ylabel('Intensity');
        xlswrite(filename,L,'Sheet1',xlRange)
        %clf
        fig = figure(2);
        plot(d2I)
        title('2nd derivative WRT position')
        jpeg = sprintf('d2I%d.jpeg',n);
        saveas(fig,jpeg);
        xlRange = sprintf('A%d',n+1);
        xlabel('Position');
        ylabel('Intensity');
        xlswrite(filename2,d2I,'Sheet1',xlRange)
end
```

B

VI CODE

The following code was used to garner the data taken by the VI probe. The VI probe took data over multiple pulse cycles; the following code compiles the data into one pulse cycle.

```
clc
% Init
close all
clear all

% Constants
PulseRate = 500; % Hertz
tp = 1 / PulseRate;
VIDataFilenameOut = input(sprintf('Please...
    input file name to print to (.csv):'),'s');

% VI Probe Data
VIDataFile = input('Please input file name to run (.csv):','s');
```

```
VIData = csvread(VIDataFile,10,0);
V = VIData(:,17);
iSV = find(V > -0.01, 1);
V = V(iSV:iSV+999)
I = VIData(iSV:iSV+999,18);
Zp = VIData(iSV:iSV+999,19);
Zm = VIData(iSV:iSV+999,20);
ts = (VIData(iSV:iSV+999,23)-VIData(iSV,23)) / 1000;
% ts = VIData(iSV:iSV+999,24) / 1000;

% Produce the modulus of the pulse rep rate with respect to...
 the sampled waveform
tm = mod(ts,tp);
[X,Ind] = sort(tm);

% Sort the data
tmm = tm(Ind);
Vm = V(Ind);
Im = I(Ind);
Zmm = Zm(Ind);
Zpm = Zp(Ind);

% Save new data file
csvwrite(VIDataFilenameOut,[tmm Vm Im Zmm Zpm]);
```